STRUCTURAL AND NANOHARDNESS BEHAVIOR OF LOW ENERGY, HIGH FLUX NITROGEN IMPLANTED AUSTENITIC STAINLESS STEEL

A Thesis Submitted to
The Graduate School of Engineering and Sciences of
İzmir Institute of Technology
In Partial Fulfillment of the Requirements for the Degree of

MASTER OF SCIENCE

in Materials Science and Engineering

by
Refika DAL

June 2018
IZMİR

We approve the thesis **of Refika DAL**

Examining Committee Members:

Prof. Dr. Orhan ÖZTÜRK
Department of Physics, İzmir Institute of Technology

Assoc. Prof. Dr. Mücahit Sütçü
Department of Material Science and Engineering, İzmir Kâtip Çelebi University

Assist. Prof. Sinan Kandemir
Department of, Mechanical Engineering, İzmir Institute of Technology

05 June 2018

Prof. Dr. Orhan ÖZTÜRK
Supervisor, Department of Physics,
İzmir Institute of Technology

Prof. Dr. Mustafa M. DEMİR
Head of the Department of
Materials Science and Engineering

Prof. Dr. Aysun SOFUOĞLU
Dean of the Graduate School of
Engineering and Sciences

ACKNOWLEDGEMENTS

To begin with I want to express my immense gratitude to my advisor Prof. Dr. Orhan Öztürk. I feel always assured that his instruction, incentive, advice, patience and teaching helped me from beginning to end.

I would like to thank Prof. Dr. Don L. Williamson and his research group from the Department of Physics, Colorado School of Mines for providing N implanted 316 stainless steel specimens and carrying out the implantation processes.

Other than that, thanks goes to staff of Material Research Center of Izmir Institute of Technology for their assistance during my studies I would like to thank Department of Dokuz Eylül University Electronic Materials Manufacturing and Application Center for facilitating Nanoindentation analysis in their laboratories and Dr. Metin Yurddaşkal for his help during analysis.

I also would like to thank my colleague and friend Özgün Karataş. Her invaluable help and support mean a lot to me during my study.

Finally, the biggest thanks goes to my mother. No words can express the encouragement she has given me.

ABSTRACT

STRUCTURAL AND NANOHARDNESS BEHAVIOR OF LOW ENERGY, HIGH FLUX NITROGEN IMPLANTED AUSTENITIC STAINLESS STEEL

316 austenitic stainless steels (SSs) are one of the most commercial and technological alloys and extensively used in the field of defence, nuclear and biomedical applications due to its excellent corrosion resistance in abrasive and erosive environment. However, this type of steel is rather soft, and these results in poor durability, in particular when this material (316 SS) is in contact with other surfaces. In addition, 316 SS is nonmagnetic at room temperature.

In order to make the surface of 316 SS harder, nitrogen ion beam implantation and wear resistant method is applied. Earlier studies of high dose nitrogen ion implantation into the surface of austenitic SSs around 400 °C substrate temperature showed that an expanded austenite phase (The Nitrogen phase in the FCC lattice of 316 SS) gives excellent wear resistance with high hardness value.

In this study, type 316 stainless steel (SS) was implanted with low energy (700 eV), high flux (2.9 mA/cm^2) nitrogen ions at 400 °C substrate temperature in order to harden its surface. Microhardness and nanohardness measurements were carried out on the nitrogen implanted surface and on the nitrogen implanted cross-section under the applied loads ranging from 6 mN to 30 mN. Both microhardness and nanohardness data suggest that the hardness of the N implanted 316 SS significantly increases compared to the hardness of the substrate material (by a factor of 3 to 4).The hardness increase is believed to be due to the high amount of nitrogen, the thick nitrogen implanted layer and macroscopic residual compressive stresses, the formation of which is verified by $\theta/2\theta$ XRD scans as lattice expansions about 10 at. %. SIMS profiles suggest concentration-dependent diffusion behavior for the N implanted layers. Based on SIMS and SEM/EDX data, nitrogen implanted layers are 4-5 micron thick and constituting about 28 %.

ÖZET

DÜŞÜK ENERJİ, YÜKSEK AKIDA NİTROJEN İMPLANTE EDİLMİŞ AUSTENİTİK PASLANMAZ ÇELİĞİN YAPI VE NANO SERTLİK DAVRANIŞI

316 östenitik paslanmaz çelikler endüstride ticari anlamda çok bulunan ve teknolojik olarak önemli alaşımlardan biridir ve aşındırıcı ortamdaki mükemmel korozyon direncinden ötürü savunma, nükleer ve biyomedikal uygulamalar alanında yaygın olarak kullanılmaktadır. Bununla birlikte, bu çelik türü oldukça yumuşaktır ve bu malzeme (316 SS) diğer yüzeylerle temas halindeyken yüzeyi aşınmaya karşı zayıf bir davranış gösterir. Ayrıca, 316 SS oda sıcaklığında nonmanyetiktir.

316 SS sert yüzey yapabilmek için nitrojen iyon demeti implantasyonu ve aşınmaya dirençli bir yöntem uygulanmaktadır. 400 ° C taban sıcaklığı civarında östenitik paslanmaz çeliklerin yüzeyine yüksek dozlu azot iyonu implantasyonu ile ilgili daha önceki çalışmalar, genişletilmiş bir östenit fazının (γ_N - 316 SS FCC kafesinde azot fazı) olduğunu göstermiştir. Mükemmel aşınma direncine sahip ve yüksek sertlik değerine sahip form elde edilir.

Bu çalışmada, yüzeyini sertleştirmek için 316 paslanmaz çelik 400 ° C sabit sıcaklığında düşük enerji (700 eV), yüksek akı (2,9 mA / cm^2) azot iyonları ile implante edilmiştir. Azot implante edilmiş yüzey üzerinde 6 mN ile 30 mN arasında değişen yüklerin altında enine kesit numune üzerinde mikro sertlik ve nano sertlik ölçümleri yapılmıştır. Hem mikro sertlik hem de nano sertlik verileri, N implante 316 paslanmaz çeliğinin sertliğinin, implantasyon yapılmamış 316 paslanmaz çeliğin sertliğine (3 ile 4 kat) göre önemli ölçüde arttığını göstermektedir. Sertlik artışının yüksek miktarda azot, kalın azot implante edilmiş tabaka ve makroskobik kalıntı basma gerilmelerinden kaynaklanmaktadır, bunun oluşumu, yaklaşık % 10 da kafeste genişleme meydana getirdiği θ/2θ XRD taramaları ile doğrulanmıştır. SIMS profilleri, N implante edilmiş katmanlar için konsantrasyona bağlı difüzyon davranışını göstermektedir. SIMS ve SEM/EDX verilerine dayanarak, azot implante edilmiş katmanlar 4-5 mikron kalınlığındadır ve yaklaşık % 28 oranında içerir.

By Osho

Now I understand why nothing was happening.
The very effort was the barrier,
The very ladder was preventing,
The very urge to seek was the obstacle.

TABLE OF CONTENTS

LIST OF FIGURES

LIST OF TABLES

CHAPTER 1

INTRODUCTION

Stainless Steels are considered to be one of the most functional materials in industry, architecture and daily life. Steel is an alloy consisting of iron and 0.05 % - 2.1 % carbon. Unlike Steel, Stainless steel has wt. % at 10.5 % chromium. Stainless steel (SS) as a schematic is shown in Figure 1.1. The role of Cr in SS is to provide corrosion resistance. The Cr reacts with oxygen to form a native oxide (Cr_2O_3) layer, approximately 5 nm thick on the surface of stainless steel giving it a corrosion resistance.

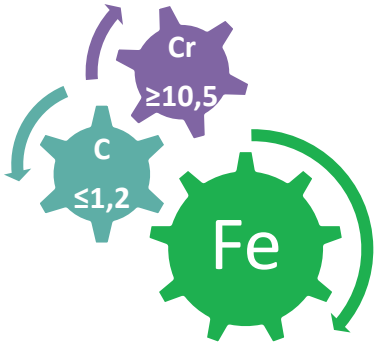

Fe + C = Steel

Fe + C + Cr = Stainless Steel

Figure 1.1. Notation of the compositions of Stainless Steel with basic elements

The focus of this study is 316 Austenitic Stainless Steel (SS) and its standards are illustrated in Table 1.1. It is a form of an alloy with Cr, Ni and Mo fundamentally. Chromium and Molybdenium are used for intensification and escalation of corrosion resistance [1]. 316 SS has a face centered cubic crystal structure where Fe, Cr, Ni atoms are randomly distributed. This material is nonmagnetic at room temperature.

Table 1.1. International Standards of 316 Stainless Steel (SS)

Chemical composition	AISI/SAE No.	DIN EN No.	JIS No.	AFNOR No.	B.S.I. No.
X5CrNiMol7122	316	1.4401	SUS316	Z6CND17.11	316S16
X5CrNiMol7133	316	1.4436		Z6CND17.12	

316 SS has a large variety of applicable utilizations in industries. For instance, 316 L (L refers to much lower C content) is extensively used in medical technology such as stents. In this thesis, 316 SS is used since as a metallic biomaterial, it has powerful and outstanding properties as compared to other types such as; ceramics and polymers. 316 SS is able to tolerate the tensile stresses due to dynamic natures. Alloys are widely used as convenient and pertinent framework material due to their desirable bending fatigue strength. Commonly, metallic types are applied in skeletal reconstructions to burden high loads. As an illustration, hip and knee endoprosthesis, plates, screw, nail, dental implants. They play an important role in developing functional devices without load; such as pumps, valves and heart pacemakers and conducting wires.

The biocompability of metallic materials are based on passive oxide layer on the surface of materials and it repairs the damage immediately. This protective layer surrounds tissue over time. Hence, chemical bonding comes into existence between the implant material and tissues like bond and hydroxyapatite. Especially, stainless steel and cobalt-chromium base alloys possess such a passive and extremely inert oxide layer [2].

Nowadays, 316 SS is being applied as pincettes, scissors, and drills in medical applications shown in Figure 1.2 [3]. In the past, bone plate, stent and artificial joint implants were performed with 316SS [4]. However, concentration of Ni, Co and Cr was found at higher levels in organs of experimental animals after sixteen weeks [5]. Immediate consequences were loosening prosthesis and/or allergic reactions to Cr, Co or Ni [6].

a b

Figure 1.2. Usage of 316 Stainless Steel; tweeze (a), stent (b) [3]

On the other hand, metallic ingrowth operation was studied with 316L stainless steel by implantation of miniplates to the legs of animals fixed by screws. After removal

from the body, these implant systems were examined using fluorescence microscopy. Inadequate new bone formation was observed adjacent to the surface of plates and screws inadequately. In addition, granulation tissue was found to be in close contact to the surface of bone which leads to loosening of implants [5-7].

Furthermore, 316 SS is an extensively practical material in industry apart from biomaterial applications such as wear-resistant bulk and hard facing materials [8-10] . For instance, it is used in marine environments (spindle, ball-valves, butterfly valves, and valve seats), chemical industry (safety valves), bearings, and bushings, sleeves, cutting tools, machine components and molding dies [8-12]. When abrasive machining is performed, physical and chemical erosion takes place. For that reason, the improvement of surface properties has been needed to be created and to develope the life-time and durability against the abrasion, wear and corrosion [8-10] for whole applications.

One of the impeding problems with 316 SS is the fact that this material is comparatively quite soft [13] and this turns out to be more significant when the surfaces of these materials are in contact or when they are in relative motion with respect to each other. In order to harden the surface of 316 SS type materials, surface modification techniques need to be applied. Previous studies showed that the various surface modification mechanisms have been able to be enhanced to resist wear and corrosion of austenitic stainless steel alloys with different thermochemical and radiation techniques [9-15]. Traditional practice for the treatment of surface properties of steels is implemented using carbon and nitrogen gasses with temperature above 500 °C. It is called nitriding, carburising and nitrocarburising. However, two problems are revealed during these treatments: Firstly, diffusions of nitrogen and carbon atoms are difficult because of the native passive layer. Secondly, nitrogen and carbon react with chromium to produce carbides/nitrides [15].

Moreover, the structure in parallel with properties of material can be altered by radiation using ions, electrons, and beams. The most popular one is nitrogen enhancement which immerses onto the surface [14]. Especially, nitrogen-ion implantation and plasma nitriding are well known [8-15]. The plasma/implantation techniques solve impenetrability of the oxide layer. The expanded austenite structure can be achieved when high amounts of nitrogen atoms are dissolved in stainless steel below 450°C without nitrides. The nitrogen atoms are located in the octahedral

interstices of the FCC lattice [10-16]. Typically, the nitrogen content ranges from 20 to 30 % after using the implantation process in an expanded structure [16-19].

In ion implantation, improvement of the tribological properties of stainless steel was studied with high dose at a 60 keV and 400 °C and nitrogen atoms are ionized [3] on 304 SS to produce a metastable and high N phase, γ_N, also called S-phase in the implanted layer [8-16].

S-phase, which is same both γ_N phase and expanded austenite phase of 304, 310, 316 SS is metastable and was discovered for the first time by Zhang and Bell, November 1983 [10-20]. Nitrogen atoms gravitate towards chromium due to developing CrN [16-23] at high temperature because of the strong affinity [10-19]. Morphology research shows as high dose nitrogen implantation at elevated temperatures, wear resistance increases progressively. However, precipitation of chromium nitride CrN can be seen and corrosion resists behavior decreases [8-24]. For that reason, it is essential that low temperature treatment is suggested and it is found that Cr atoms have low mobility and cannot obtain a precipitation structure with N at low temperature and long exposure times. In that case, N is located to provide an interstitial solid solution in the host structure which involves Cr on the γ_N layers [8-25].

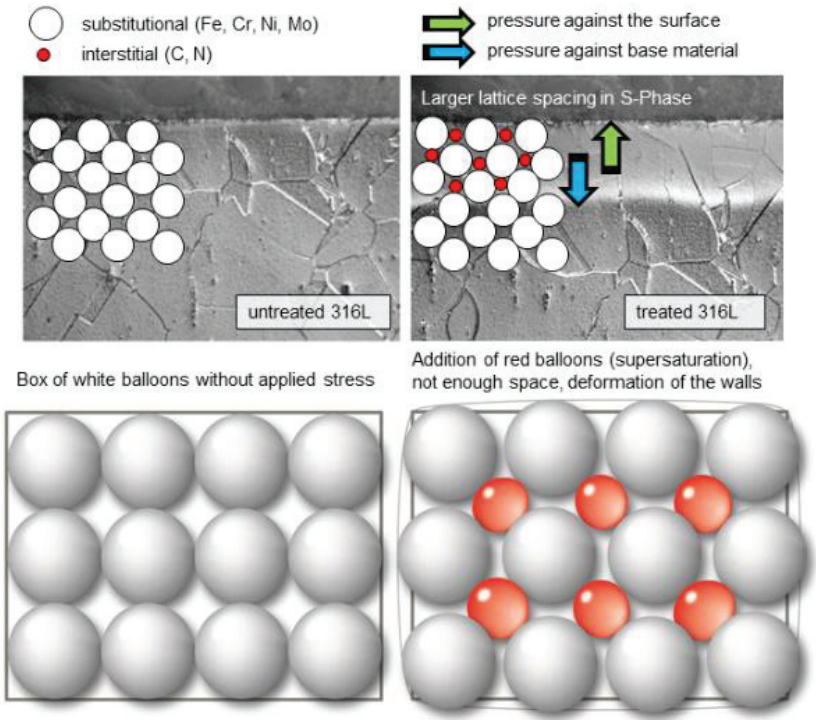

Figure 1.3. Notation about atom correlation of untreated and nitrogen treated 316 SS [26]

The terms “expanded austenite” and “S-phase” are formed by a supersaturation of the nitrogen (Figure 1.3). The implantation of the element result is easily identifiable by a bright white layer and can be attributed to lattice expansion while the core material constrains the expansion. In Figure 1.3, the nitrogen atoms impact into the interstitial spaces of the lattice and stress occurs through the surface while the base material absorbs the expansion.

Previous studies indicate that the N implantation process significantly hardens the treated surface [3]. Microhardness values show an increase as high as 20 GPa after implantation under the low energy and high flux conditions [25-28]. Similar studies show that hardness values up to 1700 HV due to an enhanced stacking fault density in the phase [7-29].

Another important issue is a sputtering effect with increasing energy, intensity and implantation time. Some investigations were done to improve surface hardening using the nitriding process. As a result of the research, ion energy was detected to be above 100 eV, and considerable erosion actualizes on the nitrogen diffused layer depending on the process time and current density [30]. For that reason, the control of N diffusion parameters is very important to avoid sputtering and loss of surface hardening during nitrogen enrichment. Nano indentation is a very sensitive method for understanding the sputtering effect on the surface hardness.

The understanding of nitrogen treatment parameters is very important issue as mentioned above. The studies which have been done comparing hardness for different timing results. An unexpected consequence, was that the hardness profile of ion implantation for 8 hours was that there was not too much difference from samples treated for 1 hour [30]. Moreover, an investigation of the effects of ion energy and current density parameters showed that ion energy is much more effective than current density on hardness level due to the sputtering .The process was implanted at 1 keV harder than 1.5 keV because of surface erosion [30].

Other ion beam implantation processes were done with a Kaufman type ion source of 300 – 400° C. Ion energy and flux were 1000 eV and $3x10^{15}$ ions cm^{-2} s^{-1}. The process was carried out at different time intervals; 5, 7 and 30 min. This study was performed to understand magnetic nature of the expanded structure. As a result, ferromagnetic patterns were obtained. This information provided potential use in new application areas such as magnetic sensor and recording media [31].

As an implantation process, the plasma and ion type were mentioned before. Another type is the plasma immersion ion implantations that increases the hardness and wear resistance [32] like plasma and beam ion methods. According to the experiment, 8% lattice expansion can be seen below 450 °C. When the lattice expansion enormously scales up, internal residual stress is higher than the yield strength. It causes plastic flow onto the outer surface zone. This result shows that the treated region is really brittle crack and fracture resistance decrease [32].

Among many methods for nitriding of steel; broad beam low energy ion implantation (LEII) is most industry-friendly method because of low voltage requirements. AISI 304 which is the same ballpark material for the AISI 316 was used for this experiment whose ion beam energy was between 110 and 200 eV. Nanohardness measurements showed that the hardness of the nitrogen treated surface layer was 4 times higher in comparison with the base material [33].

The pioneer study and application of the nano indentation method first emerged in 1992 by measuring the hardness and elastic modulus [34]. This technique has many advantages, unlike alternative probe microscopy. Firstly, characterizations are done at different areas on the material easily. Secondly, it can evaluate the properties of material at different depths.

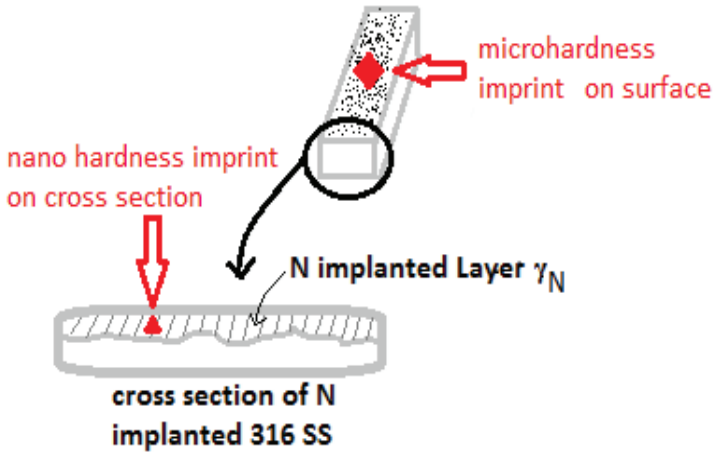

Figure 1.4. Schematic notation of imprints for microhardness on surface and nano-hardness on cross section.

The focus of this study is to investigate the hardness behavior of nitrogen implanted layers on 316 SS. Specifically, the nitrogen implanted phase will be formed on the surface of 316 SS by a lower energy, high flux N implantation technique around a substrate temperature of 400 °C. Then, microhardness and nanohardness

measurements were carried out on the N treated surfaces. Microhardness was accomplished on the N implanted surface and also nanohardness will be done on the cross section. The experimental schematic is illustrated in Figure 1.4. Surface microhardness of the Nitrogen implanted 316 SS materials were measured by Fischerscope Vickers tester. Nanohardness measurements carried out on the cross sections of the nitrogen implanted samples were performed by IBIS nanoindentation system. When hardness measurements are done from the surface, the tip of the indent may exceed the treated layer and bear down on the substrate. Results may combine the effects of the N implanted layer and the substrate that is called “substrate effect” [35].

There are two reasons that nano indentation on the nitrogen implanted layer cross section has been used. Firstly, measuring hardness on the cross section avoids the substrate effect. Secondly, since the N treated layers are usually under compressive stress, measuring nanohardness on the cross section also avoids the contribution of the stress to hardness value. Hardness measurement is done on the sample. Surfaces may get contribution from the stresses in the layers. However, nano indentation measurements on the treated layer cross sections requires a highly polished surface (i.e. low roughness). In this thesis study, the cross-sectional sample preparation is the major part.

In addition, the implantation process is a very appealing process. While ions which have high mobility diffuse in the substrate, the crystal lattice can be expanded and compressive stress occurred from substrate to surface due to large crystallites - so called “hillocks” [36]. The surface roughness increases after implantation. There are many grooves on the surface and the tip of the indent is affected from these microgrooves on the surface. The importance of cross section analyses is that they ignore the substrate and the stress effect. Also, a sample preparation on the surface is the most critical point. If preparatory steps are applied with much more time, the nitrogen implanted layer is reduced. Polishing step is accomplished on the cross-section more conveniently than the surface.

Finally, The crystal structures, topography, nitrogen profiles and compositional change on nitrogen implanted surfaces were examined with a combination of x-ray diffraction (XRD) and grazing incidence x-ray diffraction (GIXRD), scanning electron microscopy (SEM) and energy dispersive x-ray spectroscopy (EDX) and Secondary Ion Mass Spectrometry (SIMS) techniques.

CHAPTER 2

MATERIAL AND CHARACTERIZATION METHODS

2.1. Material: 316 Stainless Steel (SS)

Stainless steels are iron based alloys which are considered to be the backbone of industry. Stainless wording comes from the fact that this alloy contains at least 12 wt. % Chromium (Cr). The properties are modified by the addition of major elements such as Ni, Mo, and Mn.

Nickel (Ni) added is about 8% wt. and its primary function is to stabilize the austenite phase at low and high temperature. It is responsible for resilient toughness. In addition Ni increases the oxidation and corrosion resistance like Cr as mentioned before. Cr and Ni are added at a critical ratio and stainless steel becomes a heat resisting alloy.

The addition of 2-3% molybdenum which is ferrite former enhances the corrosion resistance dramatically. Especially, the pitting resistance equivalent (PRE) is improved from 8 to 26 by the increase of these atoms.

The stainless steel is classified according to the phases present in their metallurgical structure as follows: ferritic, martensitic (to involve precipitation hardening steels) austenitic and dublex steels which consist of ferrite and austenite. The Crystal structures of these steels are face centered cubic (FCC), body centered cubic (BCC) and body centered tetragonal (BCT), correspondingly. The most predominant type is austenitic stainless steels and it has a face centered cubic (FCC) crystal structure [37] and it is labeled as FCC-γ (Fe, Cr, Ni), FCC austenite.

In this study, 316 grade stainless steel (SS) was nitrogen implanted by a research group in the Colorado School of Mines. As a low carbon type 316 grade (EN 1.4436) stainless steel (SS) whose specific composition result is listed in Table 2.1 and 2.2 that has nitrogen implanted. The sample is austenitic type steel and has FCC atomic crystal structure and it is represented in Figure 2.1 which is illustrated via the Solidworks 3D CAD program. The diameter and thickness of samples are 30 mm and 4 mm respectively.

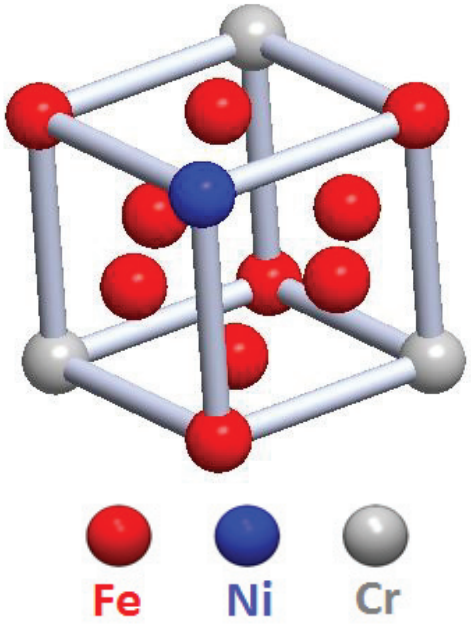

Figure 2.1. Schematic diagram of an austenitic stainless steel with FCC structure – FCC - γ (Fe, Cr, Ni)

A passive and protective Cr_2O_3 oxide layer on top of 316 SS provides a natural corrosion resistance and protects it from aggressive environments. When a heat treatment process is applied above 500 °C, sensitization occurs and carbide precipitation ($Cr_{23}C_6$) or sigma phase (Fe-Cr-Mo) is seen. Chromium depletion, which is called intergranular corrosion, takes place and the protective oxide layer gets lost at the grain boundary [38].

Table 2.1. Chemical composition (weight and atomic %) of 316 SS according to EDX result [38]

	Fe	**Cr**	**Ni**	**Mo**	**Mn**	**Si**	**Cu**	**Co**	**N**	**P**	**S**	**C**
weight %	66,39	17,07	11,64	2,16	1,66	0,35	0,34	0,26	0,07	0,03	0,02	0,01
atomic %	66,11	18,26	11,03	1,25	1,68	0,69	0,30	0,25	0,28	0,05	0,04	0,06

Table 2.2. Chemical compositions as represented by ASTM A240 and ASME SA-240 specifications are indicated in the table below.

	Fe	**Cr**	**Ni**	**Mo**	**Mn**	**Si**	**N**	**P**	**S**	**C**
weight % (max)	Balance	18,00	14,00	3,00	2,00	0,08	0,10	0,045	0,030	0,08

Although 316 SS has an outstanding corrosion properties, it is a soft material making it prone to wear. For that reason, mechanical strength to this material is provided by nitrogen implantation methods or various hardening processes. When 316 SS, whose physical properties are listed in Table 2.3, is soft then its mechanical strength is provided by nitrogen addition or a hardening process. Besides it is tough enough over a wide range temperatures and there is not a phase transformation to be seen. For that reason it is sufficiently useful for cryogen applications, because the chromium atom content is relatively high. When the temperature is increased, the molybdenum atoms tend to cause oxidation. Consequently these grade alloys are not intended to be above the 450 °C [38].

Table 2.3. Physical properties of 316 SS [39]

ASTM / AISI	**Unit**	**316**
Physical Properties		
Density	g/cm³	8.0
Melting Point	°C	1400
Thermal Expansion	m/(m K)	15.9 x10^{-6}
Modulus of Elasticity	GPa	193
Thermal Conductivity	W/m.K	16.3
Electrical Resistivity	Ω .m	0.074 x10^{-6}
Mechanical Properties		
Yield Stress	Min MPa	240
Tensile Strength	MPa	500 to 700
Elongation A50 mm	Min %	40
Hardness Brinell	HB	149
Hardness Vickers	HB	155

*In addition, 316 SS is nonmagnetic at room temperature.

2.2. Surface Treatment: Beam Line Ion Implantation

In the present study, using conventional beam line ion implantation process, whose experimental setup is illustrated in Figure 2.2, was implemented. This technique is the favorable surface treatment process, which is applied to improve tooling life and is used engineering, and biomedical applications. This technology is based on the ionization of atoms or molecules with acceleration of the electric field up to impact [40].

In this process, an ion source furnace provides the ion generation in which the nitrogen particles are evaporated and also an arc chamber in which the particles are ionized; such as N_2^+ and N^+. Then the nitrogen hits the target metal which is 316 SS by bombardments of atoms with the electrons have occurred. Because of elastic collisions a well-formed magnetic field is produced in the arc chamber. The bombardment of ions energy range is indicated from keV to MeV [40].

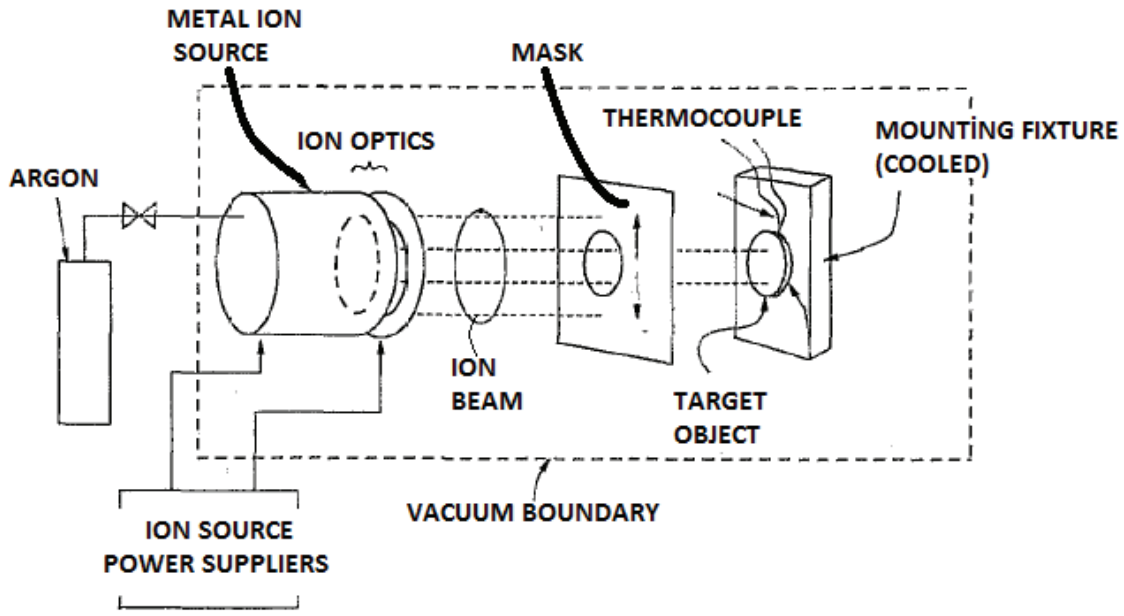

Figure 2.2. Schematic of low energy ion implanter system [41]

For this study, three samples of 316 SS discs with 30 mm in diameter and 3 mm in thickness were nitrogen implanted. The composition (all in wt. %) provided by the supplier was Fe-66.39, Cr-17.07, Ni-11.64, Mo-2.16, Mn-1.66, Si-0.35, Cu-0.34, Co-0.26 N-0.07, P-0.03, S-0.022, and C-0.013 [42]. Before the ion-beam processing, each

316 SS disc was polished to a high-quality finish. Then the samples were cleaned with chloretone and acetone to remove impurities.

Table 2.4. Chemical composition of 316 SS according to EDX results from Center for Materials Research at Izmir Institute of Technology.

	Cr	**Ni**	**Mo**	**Si**	**C**	**Fe**
weight	17,07	11,64	2,16	0,35	0,013	66,39
atomic	18,26	11,03	1,25	0,69	0,06	66,11

Before N implantation, each 316 SS disc sample was sputter-cleaned for 10 min in an Ar ion beam (1 kV, 2,5 mA/cm^2). The Cr_2O_3 passive layer was removed on surface due to nitrogen atoms can lapse easily. The treatment is illustrated in Figure 2.3. During the Ar pre-treatment time, the temperature of the sample, with the help of a substrate heater, was increased to 410 °C. The temperature was monitored by a thermocouple attached to the back of each disc. Nitrogen ion beam processing followed the Ar ion pre-treatment, and the following N beam conditions were implemented: N ion energy of 700 eV, ion beam flux of 2.9 mA/cm^2, and implantation times of 30, 90 and 240 minutes. During the N ion implantation, the sample temperature was kept at 410 ± 10 °C. Further details regarding the low-energy, high-flux N implantation into 316 SS system can be found elsewhere [42].

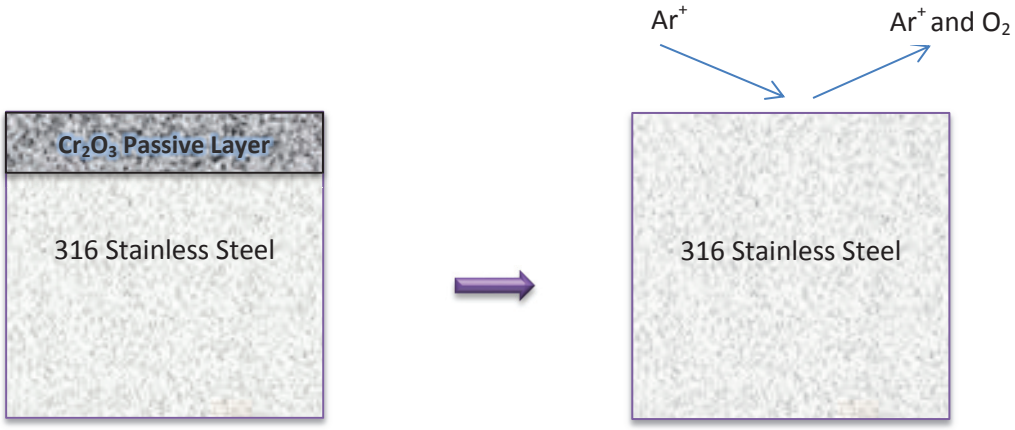

Figure 2.3. Notation of Ar pre-treatment process for 10 min, 1 kV and 2.5 mA/cm^2

2.3. Hardness Measurements

Hardness is identified as a material with characteristic and recognized abrasion resistance to permanent indentation or plastic flow. The hardness test is the most common and practical method used in all branches of engineering for the evaluation of mechanical properties which are related ductility, machinability, wear resistance and impact resistance [43]. It is used to evaluate yield strength, tensile strength, fracture toughness, the work hardening exponent, etc. [44]. In measuring hardness, an indenter is compressed into a sample or dropped onto the surface with essential loads and contact area or deformation depth of indentation is measured in traditional static hardness test.

The dynamic hardness test differs from the static one and the contact area measurement result is obtained during the indentation phase. It is an effective and advantageous measurement for the high strain rate deformation process due to cycling loads such high speed in machining applications in industry [45].

2.3.1. Dynamic Vickers Microhardness

The universal static hardness test refers to static force for giving information about strength and ductility as mentioned before. The measurement is obtained according to the resistance of the material towards plastic deformation when the hard tip penetrates the softer material. Load, indenter tip geometry and the material affect the hardness result.

In this study, Vickers hardness values (VHV) were measured on the surfaces of N implanted samples which were treated for 30, 90 and 240 min implantation times and were assessed by using a dynamic micro indenter that is Fischerscope Vickers. 100 mN test load was applied on treated surfaces constantly for a dwell time of 20 s.

The indenter is a Vickers square based pyramid shown in Figure 4.3 and it is done on a microscopic scale with a higher precision method than the standard Vickers hardness test. The recommended distance is when the center of indentation is far away twice the indentation diagonal to prohibit artificial softening [44].

The Vickers hardness value (VHV) is calculated by load divided by the contact area and estimated by the following equation [45];

$$VHV = \frac{2Psin(\frac{\theta}{2})}{d^2} = \frac{1.854P}{d^2} \quad (2.1)$$

where P is applied maximum load (kg), L is the average of the diagonal (mm) from deep sensing instrument and θ is the angle (136°) of diamond faces.

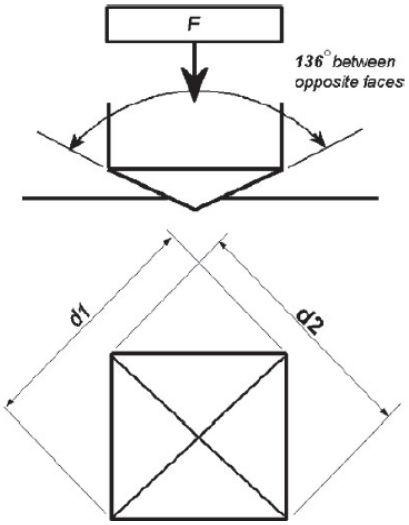

Figure 2.4. Vickers pyramid indenter [46]

The load and the penetration depth of the micro indentation mechanism is taken by a load-unload hysteresis to illustrate in Figure 2.5. The hardness value is calculated according to the traditional static hardness formula (2.1).

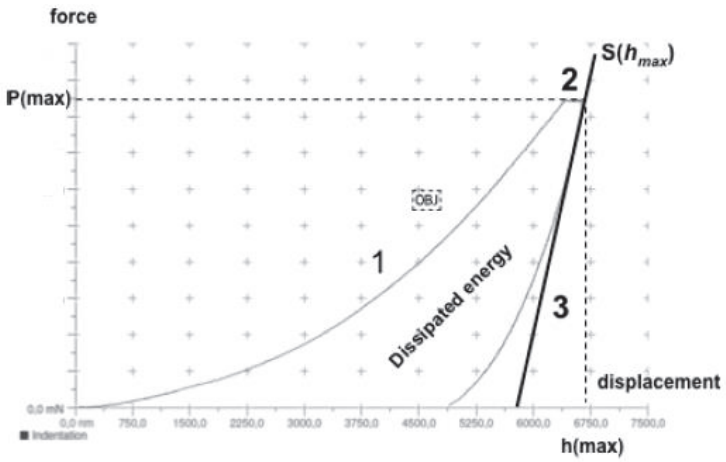

Figure 2.5. Micro Indentation hysteresis (1) Load, (2) Hold, (3) Unloading of an indenter tip [47]

2.3.2. Nanohardness Measurements

As mentioned before, nanohardness measurements were performed on the cross-section of the N implanted 316 SS sample which was processed for 240 minutes. Samples treated for 30 and 90 min could not be investigated due to thin implanted areas. This test is a sufficiently proper method which records the penetration depth of the indenter based on load for evaluating hardness according to the contact area [48]. The nanoindentation experiment is affected by tiny surface properties which are contamination, roughness, and mechanical polishing because of the indentation size [49]. For that reason scratches of the indenter tip were carefully avoided and sample preparation steps were applied.

2.3.2.1. Cross Section Sample Preparation

In this study, sample the preparation process was carried out before the indentation analysis. Polishing method was chosen because the sample surface must be really smooth due to analyzing below sub-micron level with a microscopic technique.

Cross-section sample preparation steps are shown as follows;

1. N implanted discs were cut by a water jet system as two pieces (5mmx2mmx2mm),
2. Two pairs were put into cylinder fixings,
3. Samples in the fixing apparatus were mounted with bakelite,
4. Grinding and polishing steps were applied on the surface of fixing samples.

2.3.2.1.1. Cutting: Water Jet

Firstly, the abrasive water jet technique shown in Figure 2.6 was used for the cutting operation. Although this cutting method was slower than using techniques such as plasma arcs, certain result was obtained during characterization because eroding is done as a narrow line. Because there is not a heat affected zone with the water jet method. For that reason, surface contamination, such as an oxide layer, is prevented.

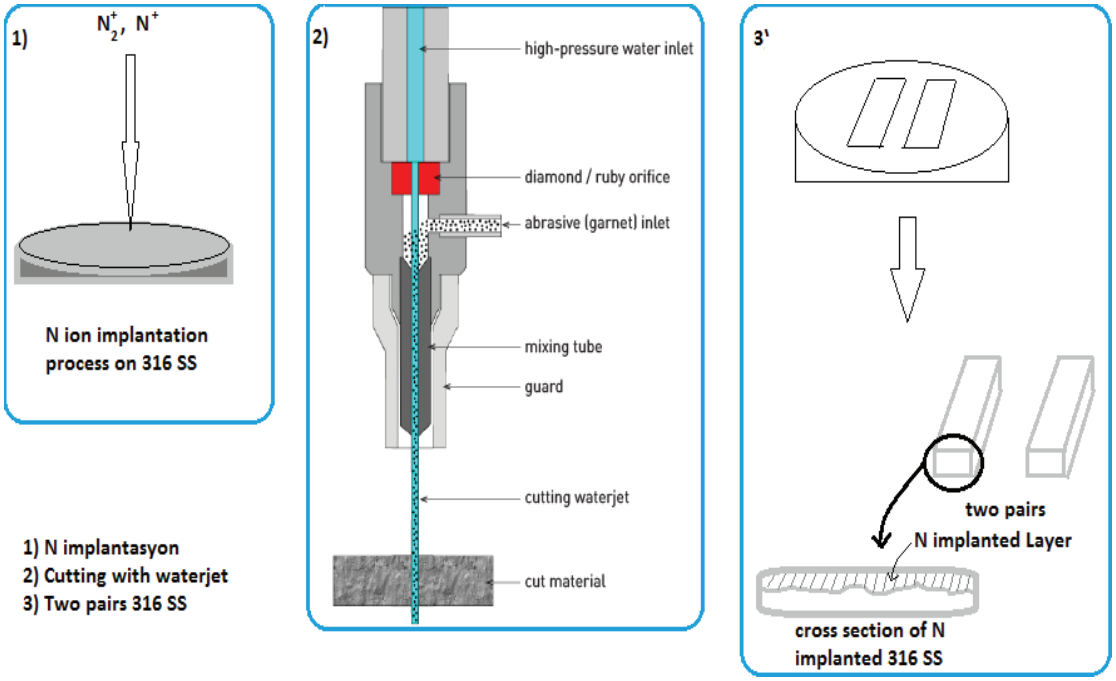

Figure 2.6. Schematic diagram of water jet cutting process [50]

2.3.2.1.2. Fixing

The sample which was implanted for 240 min was cut at the center with a water jet and cross-sectional pairs were attached. Nitrogen layer regions of pairs were placed inwardly. These cross-sectional pairs were fixed with screw in the cylinder shown in Figure 2.7.

2.3.2.1.3. Hot mounting

The hot mounting or compression moulding process was done using a Struers LaboPress-3 shown in Figure 2.8.a which was used for the handling and protection of samples. A Thermoset type which is called bakelite was used as a hard and conductive material. The Bakelite mounting process temperature and pressure were 180 °C and 250 bars and applied for 4 minutes and then cooled for 4 minutes.

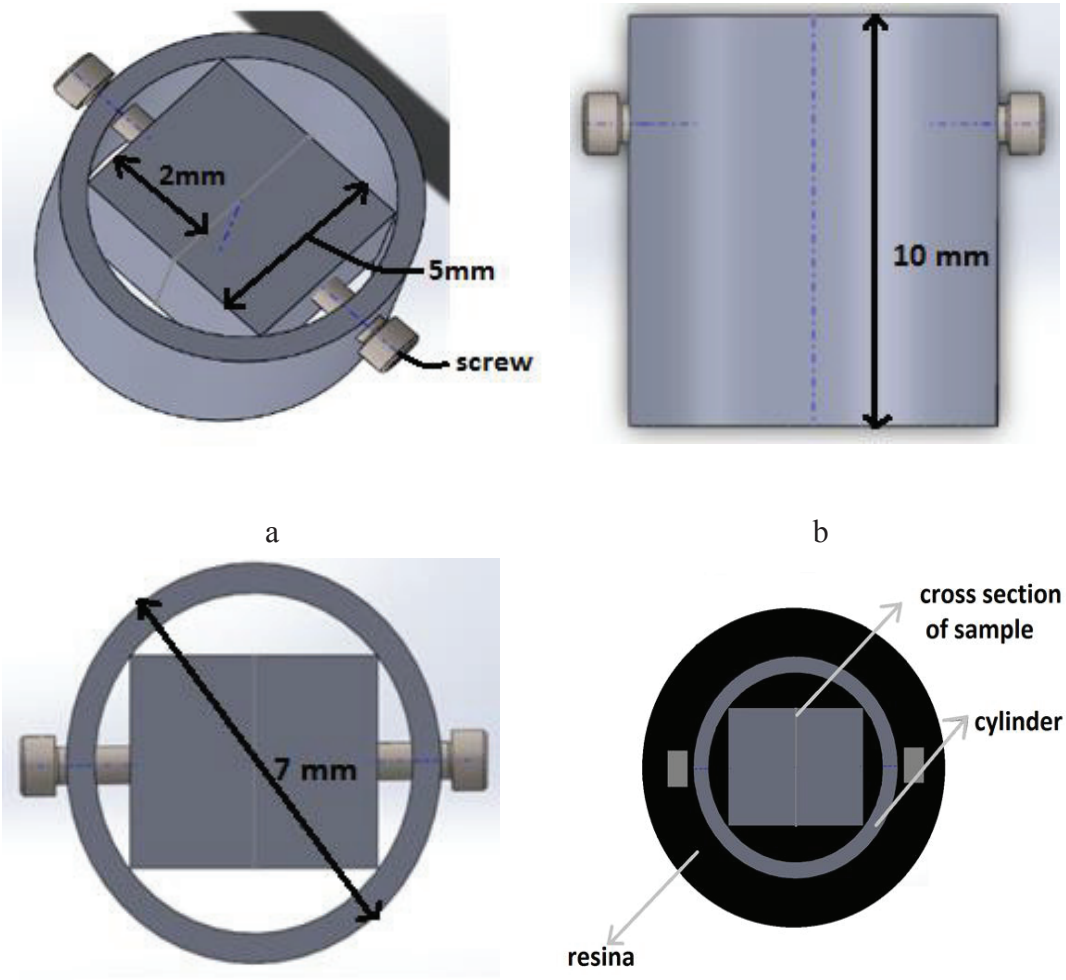

a b

c d

Figure 2.7. Samples fixing in the cylinder; 3D (a), side view (b), top view (c), samples in holder (d)

2.3.2.1.4. Grinding and Polishing

After the mounting step, the cross-section sample (Figure 2.8.b) was ground using the Buehler polishing and grinding system with abrasive SiC paper from 320 to 1200 grid size at approximately 4 or 5 N and applied 5 minutes manually as shown in Figure 2.9. Then 2400 grid size paper was used twice more than other grinding papers for obtaining a fine surface. In addition, wet grinding was used to avoid heating in order to prevent tempering and transformation [51] and mechanical surface damage was removed.

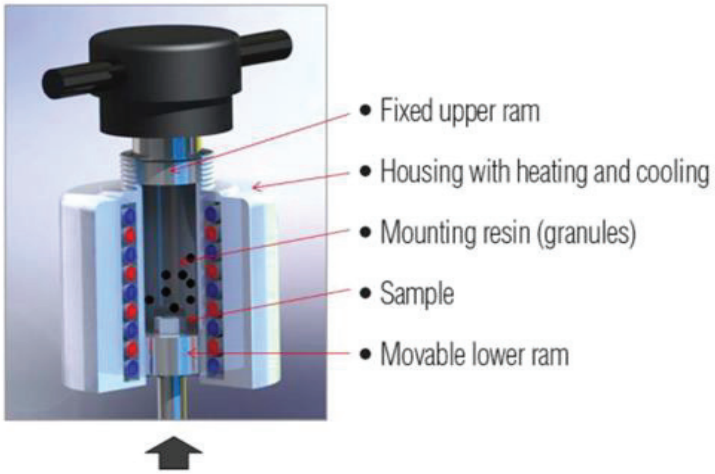

a

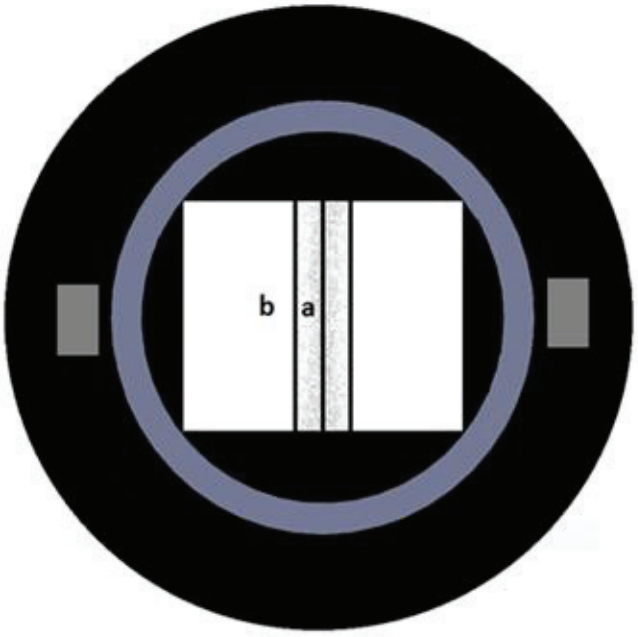

b

Figure 2.8. Schematic of mounting step (a) [52], top view of the sample after mounting (b)

Afterwards the sample was polished with diamond slurry whose particle dimensions were 9 µm, 3 µm and 1 µm (Figure 2.9.c-d) for approximately 15 minutes. After each polishing step, the sample was purified on the surface with ethanol in an ultrasonic cleaner and then it was placed in a distilled water container. Finally, a flat and mirror-like appearance was obtained. Previous experiments indicate that the roughness of the surface is approximately 10nm [13].

a

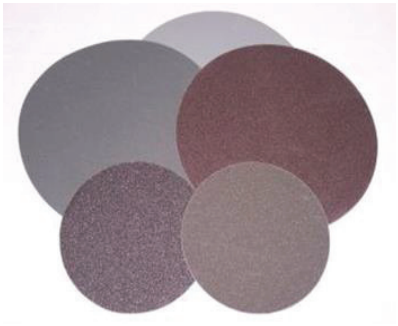

b c d

Figure 2.9. Polishing and Grinding System; polisher and grinder (a), SiC papers (b), polishing cloths (c), diamond slurry

2.3.2.2. Nano Indentation Evaluations

Smooth cross-section treated sample (Figure 2.10) was polished and measured using the IBIS Nanoindentation System shown in Figure 2.11. This was developed with CSIRO, according to Australia's national standards. This instrument is equipped to control the load and deformation of the material being tested. Measurements are provided with force and displacement sensors.

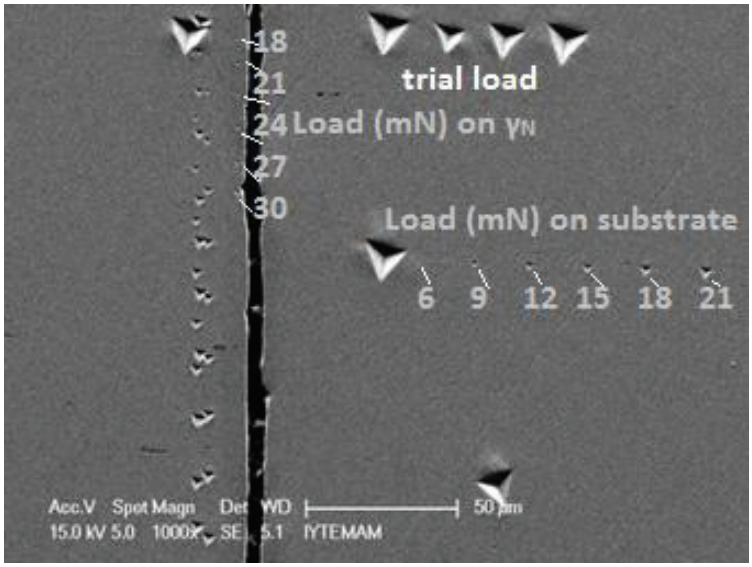

Figure 2.10. An Actual SEM image of Nano indentation tips on cross section sample

Figure 2.11. IBIS Nanoindentation System located at EMUM (9 Eylül University)

The indentation equipment comprises three components; an indenter, an actuator, and the sensor. The material of the indenter has rigid properties to transmit the force. The actuator provides the load and the sensor measures the indenter displacement.

The three sided pyramid Berkovich diamond indenter (Figure 2.12) which is the most favorable and popular, is used in these experiments. At first view, it is easier to give a single point shape and an ideal Berkovich indenter tip radius must be really sharper. However, it is not possible to achieve this for every tip. Generally the tip radius

of the tip 50-150 nm and a fine radius tip allows the contact mechanics in order to obtain correct information [48].

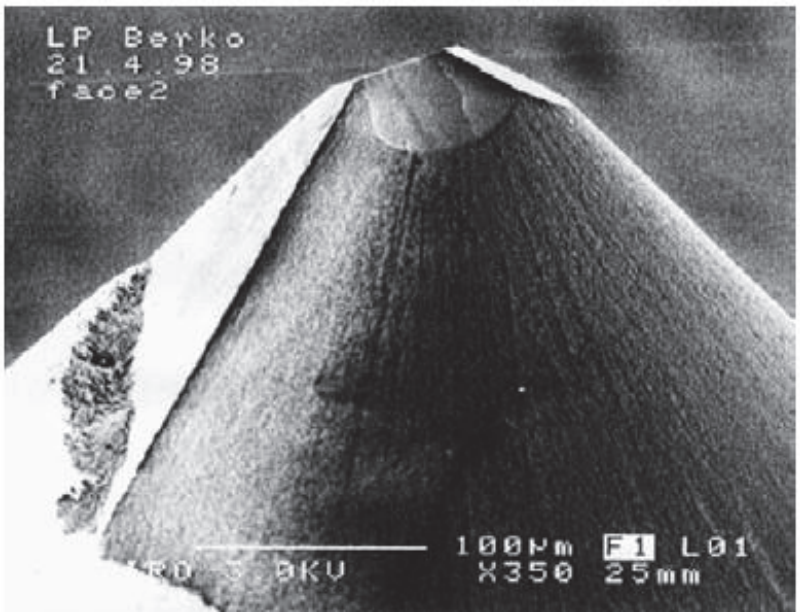

a

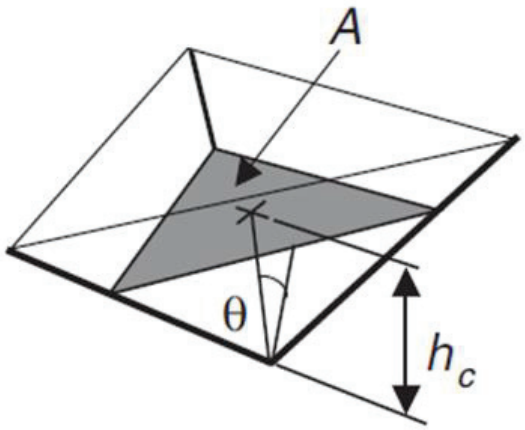

b

Figure 2.12. High-magnification SEM image of a Berkovich diamond indenter (a) and indenter geometry (b) [48]

Applied loads were 6, 9, 12, 15, 18, 21, 24, 27 and 30 mN and the load-unload data were acquired from the substrate and nitrogen layer at 240 min (Fig.2.13.) from the cross-section sample which was connected to each other, put in the cylinder and covered Bakelite, with a three-sided pyramid Berkovich diamond indenter. Samples which were treated for 30 and 90 min could not be investigated due to far thinner implanted areas than the Berkovich tip size.

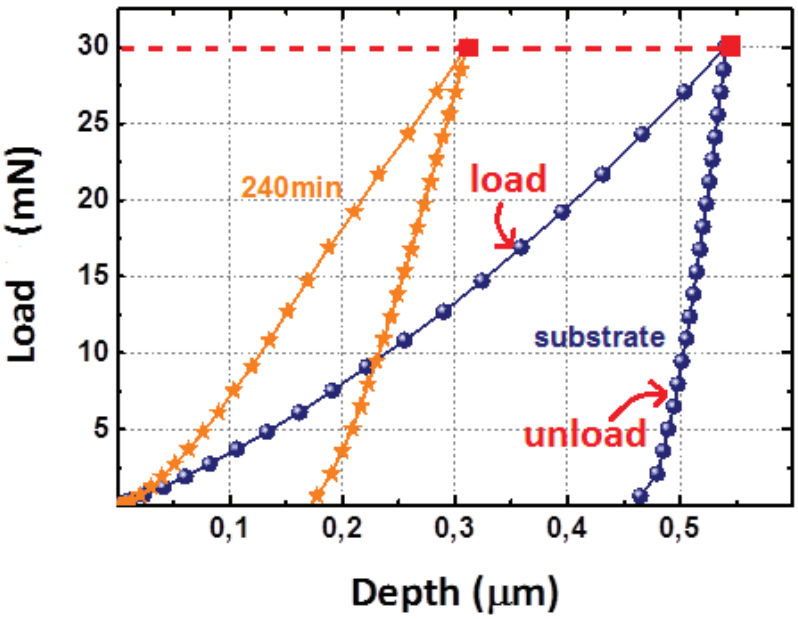

Figure 2.13. Actual nano indentation load-depth curves for 30 mN for substrate and N implanted SS

2.3.2.3. Hardness and Elastic Modulus Evaluations

The probing using a submicron characterization technique, which investigates the mechanical properties of thin film, coating and surface modification is in high demand. The advantage is that it is capable of measuring below one micron level. The data which is called load-displacement, shown in Figure 2.14, showed that loads apply and obtain depth according to force. In addition this technique is nondestructive.

Basically, the Hardness, *H*, and the elastic modulus, *E*, were measured using indentation methods. In addition, the strain hardening, index, fracture toughness, yield strength and residual stress can also be calculated which has already been mentioned regarding the information about the micro-hardness measurement, although they are not evaluated in this study. The values were obtained from data which had a cycle of loading and unloading according to Oliver and Pharr [53].

Cross-section of an indentation is shown in Figure 2.14.The total displacement is identified as h and the vertical distance is called h_c. This is also named the contact depth. h_s is the displacement of the surface at the perimeter of the contact.

$$h = h_c + h_s \tag{2.2}$$

Contact depth, h_c , is calculated and shown in Figure 2.14. and it can be noticed that;

$$h_c = h_{max} + \varepsilon \frac{P_{max}}{S} \tag{2.3}$$

Where ε 0.75 is the strain for the Berkovich indenter conical geometry and P_{max} is calculated from the load-unload curve shown in Figure 2.14.b. At peak load, the load and displacement are P_{max} and h_{max} respectively, and the radius of the contact circle is *a.* Upon unloading, the elastic displacements are recovered, and when the indenter is fully withdrawn, and the final depth of the residual hardness impression is h_f[53].

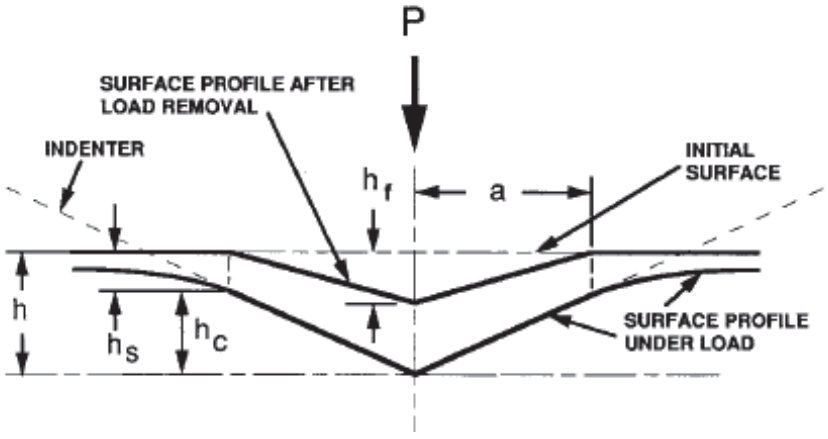

a

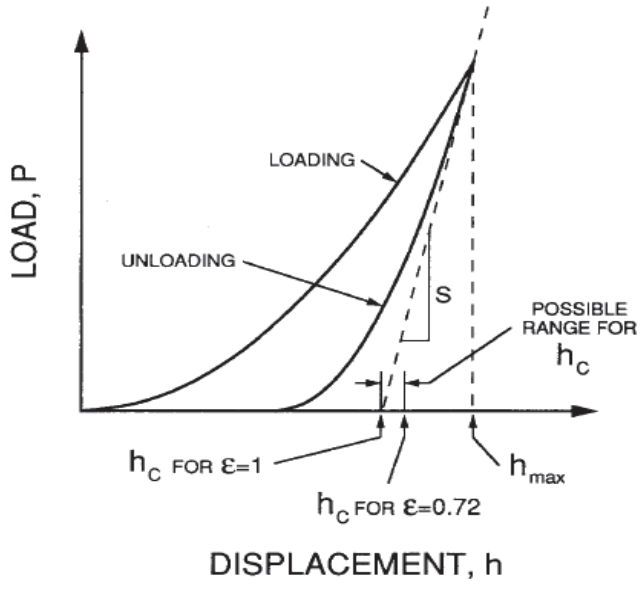

b

Figure 2.14. Schematic designation of a cross section through an indentation process (a). Actual diagram of load- unload indenter displacement showing the analysis interpretation of the contact depth (b).

In addition hardness, H and the elastic modulus, E is determined from Figure 2.14.b. Hardness, H, form is shown in the general formula;

$$H = \frac{P_{max}}{A} \tag{2.4}$$

The projected contact area, A, contact depth, h_c function for the Berkovich indenter;

$$A = A(h_c) = 24.56 \cdot h^2 \tag{2.5}$$

The effective or reduced elastic modulus, $E_{eff\ or\ reduced}$, is shown in the equation;

$$\frac{1}{E_{eff\ or\ reduced}} = \frac{1-\nu_i^2}{E_i} + \frac{1-\nu^2}{E} \tag{2.6}$$

where E and ν are Young's modulus and Poisson's ratio for the specimen and E_i and ν_i are the same parameters for the indenter.

2.4. Nitrogen Phase Analysis

In our experiment, the N implanted layer phases were examined by X-ray diffraction analysis (XRD) which is a nondestructive technique. X-ray diffraction, which is a unique method, has been used to identify fundamental compounds and phases of unknown bulk crystalline material at an atomic level such as chemical composition and crystal structure determination, layer composition and thickness determination. Basically the crystallinity of the compound is obtained by calculating the unit cell dimensions on near surface layers since x-rays are intensely absorbed when passing through the material.

In this study X' Pert Pro MRD Thin Film X-Ray Diffractometer System which was used to analyze the crystal structure of a line of the microstructure of nitrogen implanted materials. Primarily, analyzing the near-surface crystal structure of an ion implanted surface was practiced using the Gonio mode which has a θ-2θ (Bragg-Brentano) geometry design illustrated in Figure 2.15.

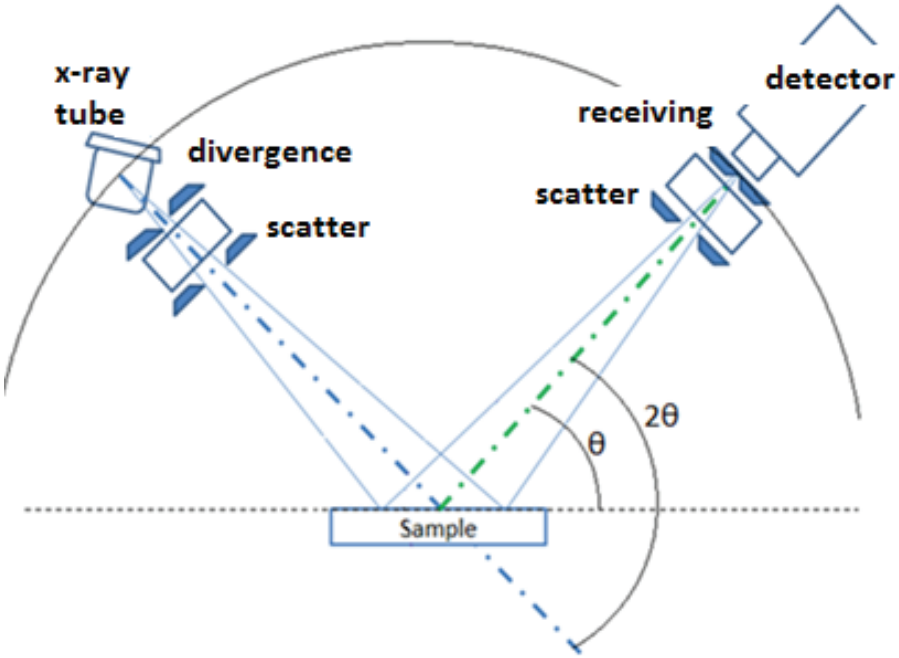

Figure 2.15. Schematic diagram of main components of x-ray diffractometer and the θ - 2θ (Bragg-Brentano) Gonio mode

2.4.1. Production of X-rays

X-rays are produced by high speed electrons colliding with a target metal form an X-ray source consisting of a cathode ray tube. The source of electrons, a voltage, and a target metal are critical elements for an x-ray tube which is water cooled to prevent melting in it. The high voltage is produced from a filament and accelerated electrons are emitted from a target metal, made of copper, cobalt or molybdenum, where they generate X-rays with characteristic wavelengths. Electrons are focused by a metal cup which surrounds a tungsten filament. Focusing occurres with the same high voltage at negative way [54]. In addition, x-rays are thrown from this focal metal cup. Some of the x-rays escape from the tube with windows which are made of aluminum, beryllium or mica.

The tube produces x-rays less efficiently and it is not sufficient for x-ray diffraction from crystals. In fact the characterization can be determined much later. The rotating-anode tube is a solution for this issue without excessive heating of the anode [54].

2.4.2. Bragg-Brentano Diffraction Phenomenon

The XRD peak position gives information after the reflection process to determine unit cell parameters using Bragg's Law [54]. Incident x-rays make a θ angle between the crystal plane of the target material. Reflections take place from the crystal plane at θ angle. As a result, 2θ angle is equal to the incident x-ray beam and reflected one. The difference of path length defined as 2d sinθ. Strong diffraction occurs which is called constructive wave interference and this difference in the path from the incident beam to the detection point is equal to one wavelength, λ:

$$2d \sin\theta = \lambda \tag{2.7}$$

Value of the wavelength depends on the diffraction angle. When θ is changed, diffraction is obtained at different plane and this condition is applied n times;

$$2d \sin\theta = n\lambda \tag{2.8}$$

When the diffraction plane is (110) for cube faces, the formula can be;

$$2d_{110} \sin\theta = n\lambda \tag{2.9}$$

In addition, interatomic distance (d_{hkl}) is calculated with lattice parameter α_0 according to Miller indices (*hkl*) are:

$$d_{hkl} = \frac{a_0}{\sqrt{h^2+k^2+l^2}} \tag{2.10}$$

In this experiment, the measurement was performed with Cu $K\alpha_1$ filtered radiation, Bragg angle scanning range is from 35° to 55° due to range is between the sample surface, incident and diffracted rays were equal. Radiation wavelenght is 1.5406 Å in θ-2θ geometry. The generator voltage was 45 kV with 40 mA for current.

Firsty, the sample was at the center of goniometer circle and surface of sample was tangential to this circle. During diffraction, sample and detector were revolved within the boundaries of the same circle. In addition, the generator was stationary in system and crosswise position to the detector. Finally, data of signals were collected and recorded from computer base system about diffraction pattern. In addition, a mirror was emplaced in alignment sample and source to increase affinity of beam collection on the sample.

2.5. Nitrogen Profiles Detection Depth

In this study, the nitrogen composition depth profiles of N implanted samples were acquired by secondary ion mass spectrometry (SIMS) for treated materials lasting 30, 90, and 240 min. This technique is an analytical method to study the composition of a treated surface. The primary ion beam energy is between 0.5 and 20 keV to focus on the surface and to generate secondary particles by sputtering during analyzing.

As the Cs^+ ions were used primary ions and sputtered neutral but a small percentage of ionized atoms could be analyzed to gain knowledge about the elemental compositions of the surface. In general, O_2^+, O^-, Cs^+, Ar^+, Ga^+ or neutrals were bombarded onto a solid to generate secondary ions [55].

Mass analyzing was performed with three different ways according to mass-ions ratio. They are quadrupole analyzers, magnetic sector analyzers and time-of-fight analyzers as in the condition of all studies. In the following step, ions are categorized by a detector to give information about mass ratio, ion image, depth profile and 3D image as illustrated in Figure 2.16 below.

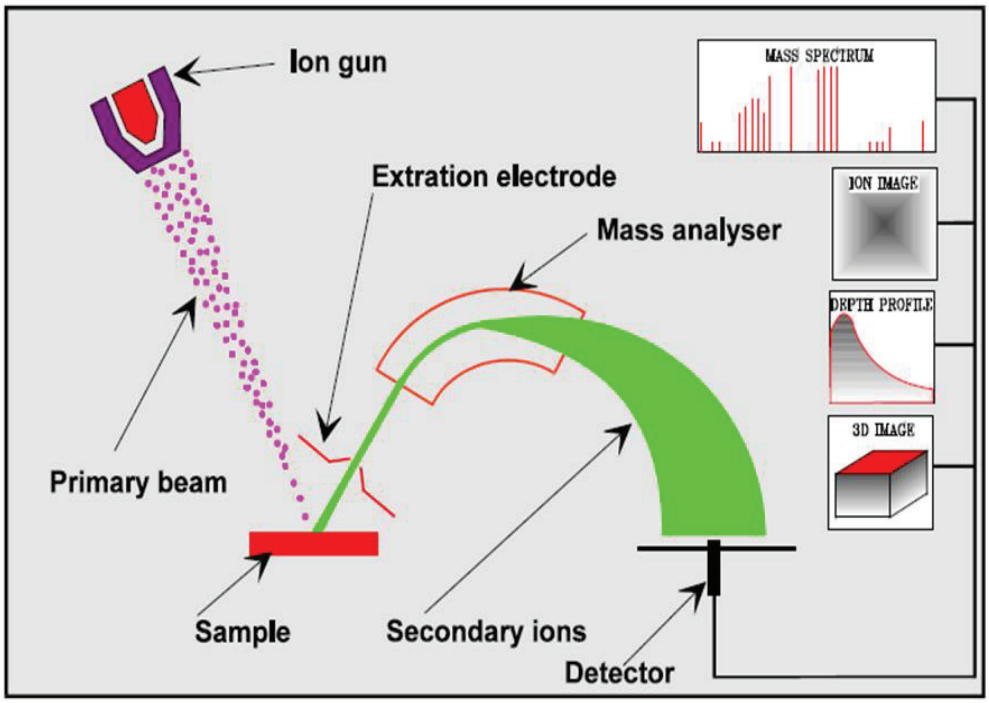

Figure 2.16. Actual structure and mechanism of Secondary Ion Mass Spectroscopy [56]

While Static SIMS permits analyzing on elemental surface, the depth distribution of element and composition information are gained in the bulk from Dynamic SIMS mode. Mass signals are obtained by eroding the surface with secondary ions. Henceforth, mass signal as a function of time is taken by recording spectra. ultimately, the linear intensity-time data is converted to intensity-depth profile.

This technique is a highly sensitive method and used for solving problems about surface contaminations. Excessively low concentrated elements which are ppm level, are analyzed with SIMS. Although depth resolution is approximately 10 nm, "matrix effect" problem can be seen during measurement due to incompatible ions sputter flux with specific element-matrix combinations. In addition, more than adequate erosion can be occured since ions sputtering.

In our work, SIMS analysis was performed using a 15 keV Ga^+ beam and a 2 keV O_2^+ beams for sputtering respectively. The goal of the experiments was to take the nitrogen depth distribution profiles of the N implanted samples.

2.6. SEM Analysis of Cross-sectional Austenite N implanted Sample

In this study, Scanning Electron Microscopy (SEM) was used for understanding surface properties of nitrogen treated part at cross-section sample with backscattered (BSED) mode before nano indentation analysis. In addition, nano indents on nitrogen implanted place were compared and contrast the dimensions with unimplanted part.

Furthermore, nitrogen distribution was investigated by using line scanning method of Energy Dispersive X-ray Spectroscopy (EDX) analysis on cross section sample which is shown in Figure 2.17.

The electron beam is scanned horizontally through the specimen in two perpendicular x and y directions. In comparison to y-scan the x-scan is faster and produced by a saw tooth-wave generator [57]. The generation is occurred at scan coils above the objective lens see Figure 2.18 as below. The electron probe moves in the straight line from A to B.

The signal is produced, when a high energy beam of electrons interact with the specimen, as a result, they lose their energy and absorbed by specimen. When accelerated electrons are scattered both elastically and inelastically; secondary, backscattered, auger electrons and characteristic x-rays are produced as shown in Figure

2.18. and they depend on the electron energy and the atomic number of the elements [57].

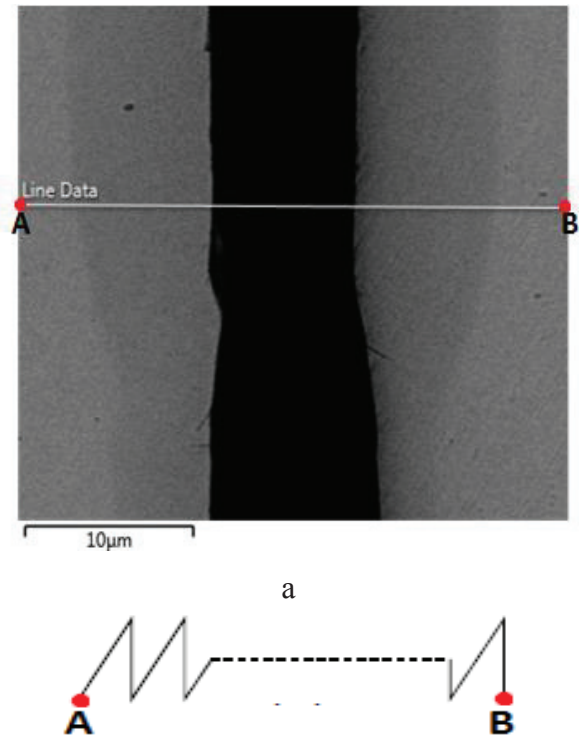

Figure 2.17. Image of the x-scan routing (a), Elements of scan: A to B (b)

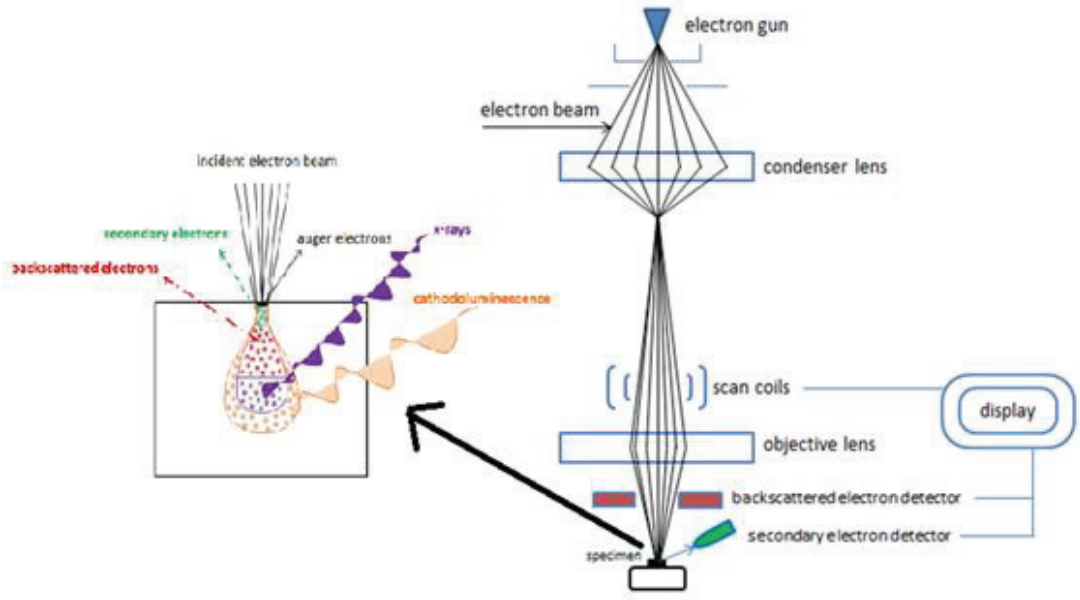

Figure 2.18. Components of SEM structure and Schematic of Electron Beam Interaction

CHAPTER 3

RESULTS AND DISCUSSIONS

3.1. Nano Hardness

In this section, Nano hardness data which is taken through the treated and untreated parts of the N implanted 316 SS sample is presented. Hardness, H, and elastic modulus, E, values were obtained from indentation load – unload curves with Oliver and Pharr approach using Berkovich indenter [52]. The data in Figure 3.1 was taken under the applied load of 30 mN. As illustrated in Figure 3.1, the N implanted layer is rather harder than the substrate. Under the same applied load, while the indenter depth for the N treated part is 0.31 mm, it is 0.54 mm for the softer substrate phase. Evaluation of the date in Figure 3.1 gives a nanohardness value of 23 GPa for the layer, while this value is ~5 GPA for the softer substrate phase. This says that N implanted layer hardness is 5 times larger than the substrate hardness.

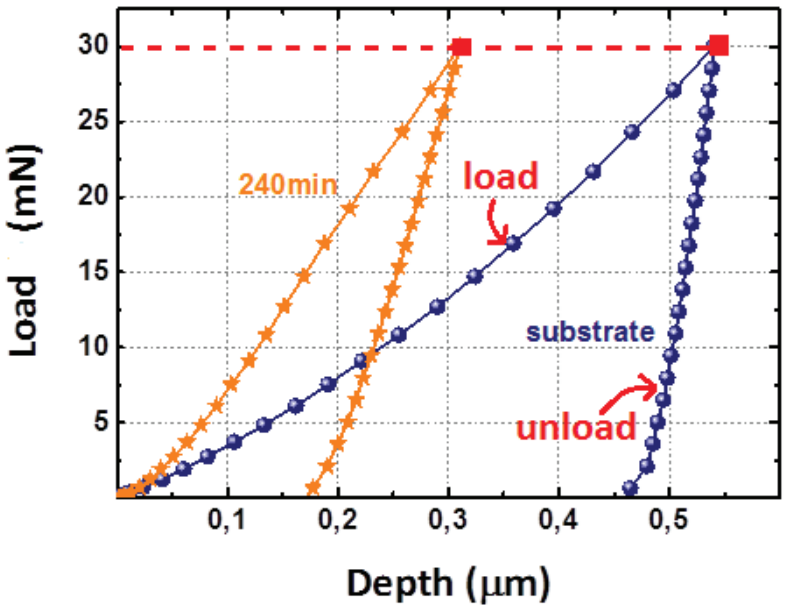

Figure 3.1. Graph comparing force-depth curves for N implanted sample at 240 min and substrate with 30 an applied load of 30 mN

The main goal for the residual SEM imprints investigation was to correlate hardness values and indent dimensions that may be observed after indentation as seen in Figure 3.2 for cross-section sample with events that occurred on the corresponding load-displacement curves in Figure 3.1. For the same load, the contact area varied in the cross-sections of 240 min N implanted layer and substrate under study. Thus, these images provide a qualitative value for the resistance of the material when it is gone down by a Berkovich indenter. The γ_N phase which is treated at 240 min had a smaller contact area than the substrate. As it can be seen from these SEM images the N implanted part is harder than the substrate phase as compared to indent sizes.

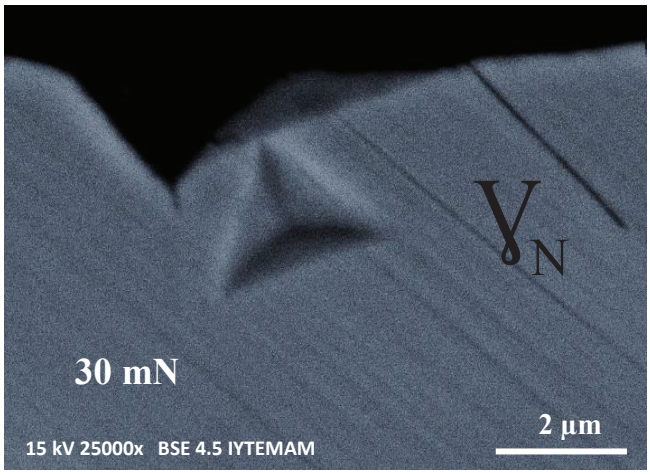

a

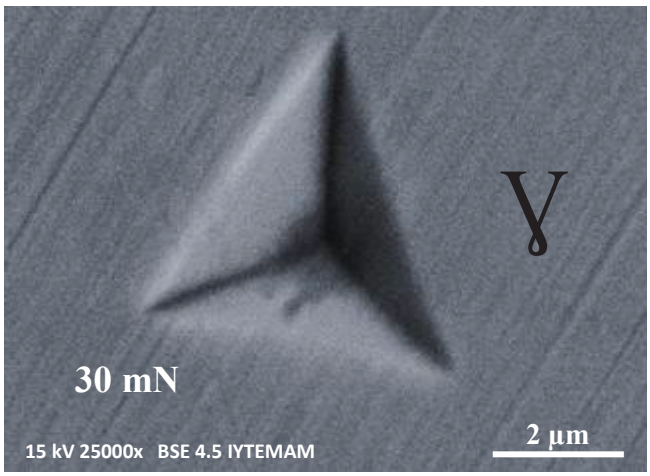

b

Figure 3.2. Residual SEM BSE images of the indentation imprints for γ_N phase (treated at 240 min), (a) and γ phase (untreated layer), (b) at a maximum load of 30 mN on cross section of sample.

The load - unload process can be measured to investigate the plastic and elastic deformation of the N implanted layer. Most materials execute a strong indentation size effect [49]. Therefore it is necessary to analyze the load dependency over a wide range of the applied indentation load. The relevant load-depth curves are shown in Figure 3.3 for all loads on N ion-implanted layer for 240 min and substrate.

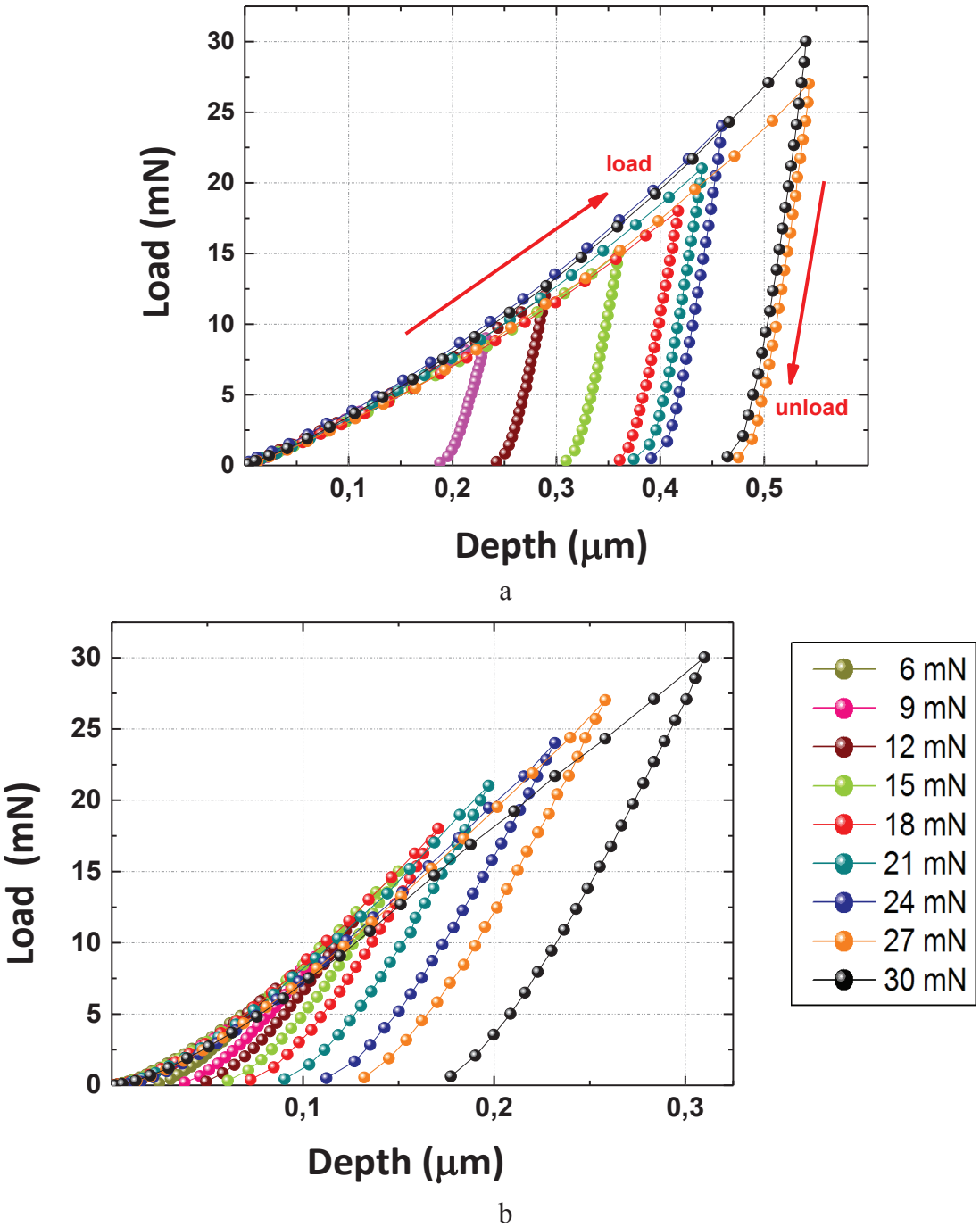

Figure 3.3. Characteristic load and unload curves under applied loads of 6, 9, 12, 15, 18, 21, 24, 27, 30 mN (a) untreated layer and, (b) N treated layer at 240 min

The traceable depth of the treated layer increases from 0.08 μm to 0.31 μm when the load ranges from 6 to 30 mN. On the other side, the depth of the unimplanted layer increases from 0.16 μm to 0.54 μm as the load ranges likewise from 6 to 30 mN. As it has been mentioned earlier the depth of soft part which is substrate is higher than N implanted part.

As it is known, many methods are applicable for mechanical local characterizations. Which are divided into nanoindentation, micro-indentation, macro-indentation and pico indentation according to the indent tip size which is described with a load-depth curve shown in Figure 3.4. These methods can be qualified in physical impact. The deformation can take place in two different ways; elastic and plastic. There is no indent at elastic type seen because of reversible and actualized at angstrom scale [58]. By increasing of the load, P, deformation type can be changed with size of distortion region. Plastic deformation rate enhanced in atomic mechanism and atoms are permanently relegated from the position. Atomic displacements produce slip plane in closed pack crystallographic structure [59]. Comparing the load depth curve, high amount of the plastic deformation is seen because of the slope as shown in Figure 3.3.a. Unlike, slightly high slope has been seen for nitrogen implanted layer which is illustrated in Figure 3.3.b

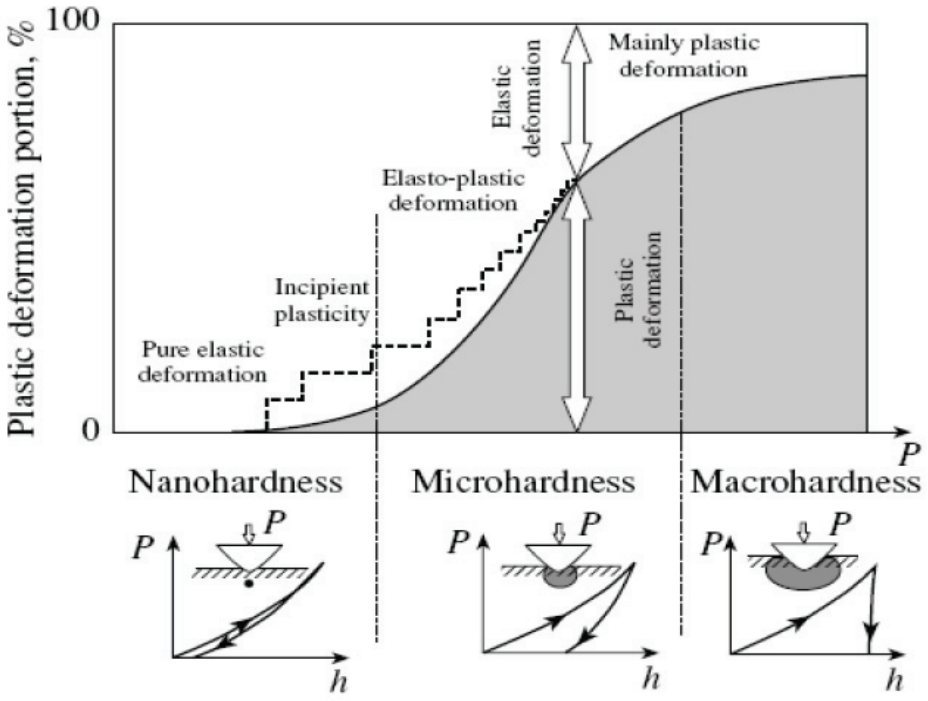

Figure 3.4. Elastic to plastic deformation with increasing indentation load [60]

Residual nanoindentation imprints at different applied loads observed by BSE-SEM contrast shown in Figure 3.5. a, The BSE images of the indentation imprints in Figure 3.5 a and b show that the size of the residual imprint rose as the applied load increased for both. In addition, there is a considerable difference in the size of the indents placed between the nitrogen implanted γ_N phase and un-implanted γ phase. When the load imprints compared under desirable and same conditions there are 5 loads which are seen at 5000 magnification in the plastic deformation band with 18 mN, 21 mN, 24 mN, 27 mN, 30 mN. Furthermore, only 3 loads are seen which are 24 mN, 27 mN, 30 mN and visible in Figure 3.5 b that the indentation size is small enough (4 μm–5 μm) at an inter-indent distance of about 15–20 μm, thus the individual indents don't influence each other.

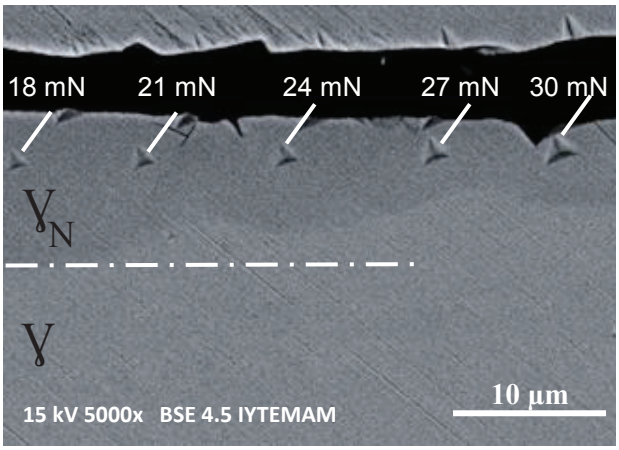

a

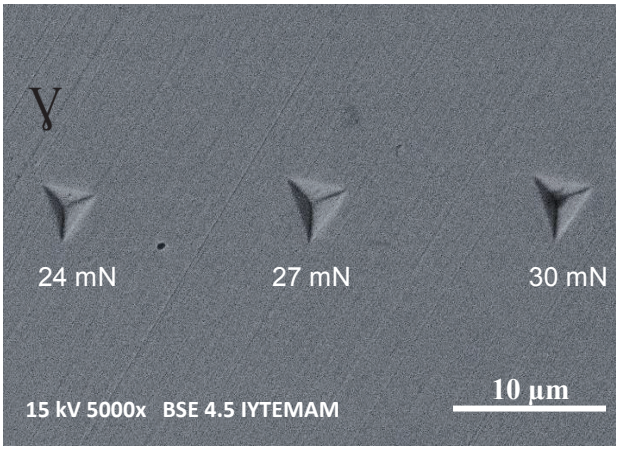

b

Figure 3.5. Residual nanoindentation imprints at different applied loads observed by BSE-SEM; (a) 18 mN, 21 mN, 24 mN, 27 mN, 30 mN onto cross section of N implanted area, (b) 24 mN, 27 mN, 30 mN on substrate.

Comparing results of cross section sample which has treated layer and substrate showed that the nitrogen implantation at 240 min increased the surface hardness approximately four times as shown in Figure 3.6. There are nine different hardness values for each part. Blue line (-▲-) determines the hardness values of substrate ranging from 4.8 GPa to 12.36 GPa. They are listed at Table 3.1. Yellow line is shown as (-▼-) and it describes the hardness values of the nitrogen implanted layer and they are between 23.26 GPa and 104.26 GPa in Figure 3.6. Actual Vickers macro hardness value is 155 HV and it is converted to 1,52 GPa. When this commercial result is compared to nano indentation result of un-implanted 316 SS, hardness of final group loads can be referenced, although the nano hardness result of final groups are higher than macro hardness result. In addition, first two loads result can be ignored due to loads which were really low and the sensitivity can be nominal.

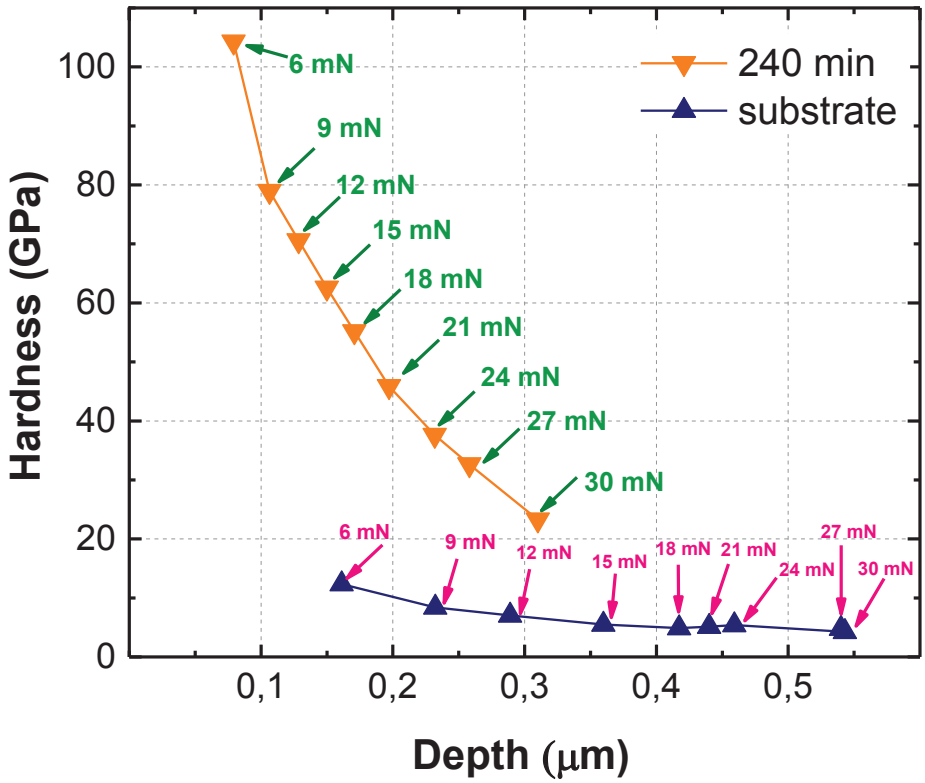

Figure 3.6. Compare data of Nanoindentation hardness (GPa) profiles between cross of N implanted layer at 240 min and un implanted 316 SS, as a function of depth (μm)

In addition, many researches have been preoccupied with the fact that the hardness can increase by decreasing the depth as illustrated at Table 3.1. There are some

noticeable influencing factors such as indenter tip radius and the contact area but also the creep property would be another important one [61].

The E values in GPa for the expanded phase structure and substrate are shown in Table 1. The test result showed minor difference between E values recorded at max load (30 mN). The E values recorded at different distance of the implant interface were plotted in Figure 3.7 which the elastic modulus is calculated from IBIS nanoindentation system according to Oliver and Pharr [53] like hardness profile. The nano indentation elastic modulus result of max load is bearing a resemblance to the commercial and un-treated 316 SS, although low loads can increase the elastic modulus by three times.

Table 3.1. Depth, Hardness and Elastic Modulus result related with loads according to Nano Indentation Test

	Depth (μm)		**Hardness (GPa)**		**Elastic Modulus (GPa)**	
Load	***Substrate***	***240min***	***Substrate***	***240min***	***Substrate***	***240min***
6	0,16	0,08	12,36	104,26	371,21	1081,19
9	0,23	0,11	8,38	78,94	320,51	802,05
12	0,29	0,13	7,03	70,59	303,53	699,44
15	0,36	0,15	5,48	62,56	291,37	622,10
18	0,42	0,17	4,89	55,18	250,99	571,53
21	0,44	0,20	5,14	45,88	265,07	489,05
24	0,46	0,23	5,39	37,61	282,82	375,93
27	0,54	0,26	4,26	32,61	248,30	343,52
30	0,54	0,31	4,80	23,26	276,08	266,24

The elastic modulus of the Nitrogen implanted layer decreases from 1081 to 266 GPa as the load ranges from 6 mN to 30 mN. Also, as shown in Figure 3.7, the decrease in the modulus is more significant for the load ranging from 6 mN to 15 mN. There are two possible reasons for this variation in the hardness:

(1) Show an alteration in the distribution and concentration of nitrogen from surface to bottom;

(2) Lattice distortion due to plastic deformation of the expanded phase layers. In addition, the treated layer can have a cold plastic deformation with increase in indentation loads. The elastic modulus could be reduced significantly reduction due to enhanced plastic deformation which correspondingly leads in structure change [62].

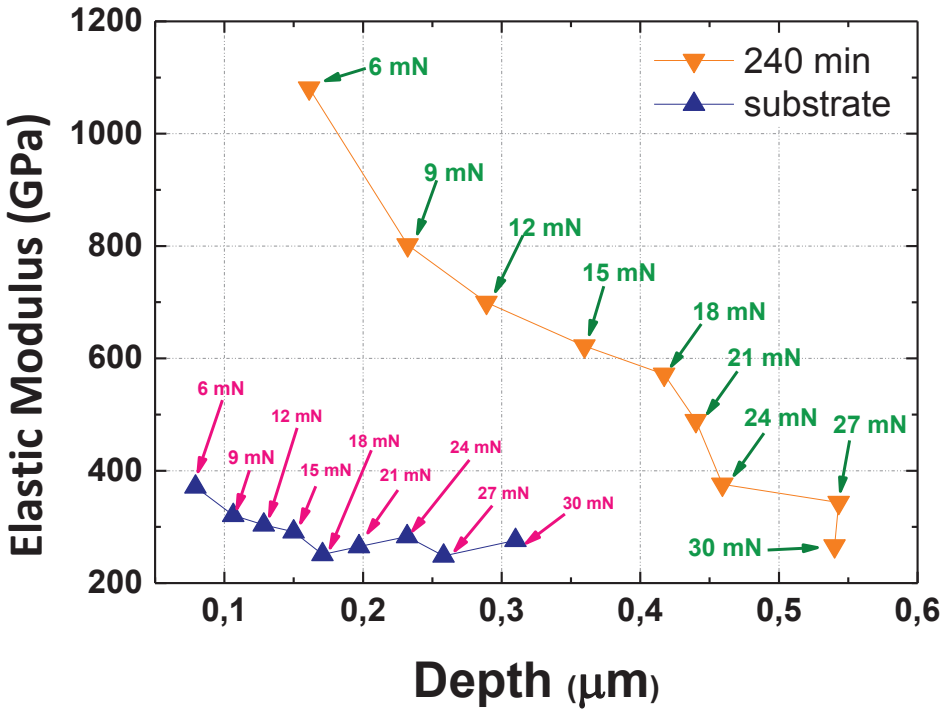

Figure 3.7. Actual data of Nanoindentation elastic modulus (GPa) profiles between cross of N implanted layer at 240 min and un implanted 316 SS, as a function of depth (μm)

3.2. Micro Hardness

Surface microhardness data is shown in Figure 3.8 for the un-implanted and N ion implanted layer at different process times which are 30 min, 90 min, 240 min intervals, the hardness increase is modest for the sample implanted at 400 °C for 30 min. However, In comparison to the untreated substrate material, the hardness increase of the nitrogen implanted material treated for 90 and 240 minutes is quite significant and two times more than untreated one.

The Vickers indenter is envisaged according to geometric structure in order to obtain the similar indentation imprints. At the first side, the hardness should be independent of the applied load and the indentation size in expectation due to the results is true for commercial macroscale test in industry. However, for microscale which is well existent that the hardness decreases or, more frequently, increases with the decrease in the applied load like nano scale shown in Figure 3.6 is mentioned above.

This effect is termed as the ‘‘indentation size effect’’ (ISE). This effect is shown in Figure 3.9 [63].

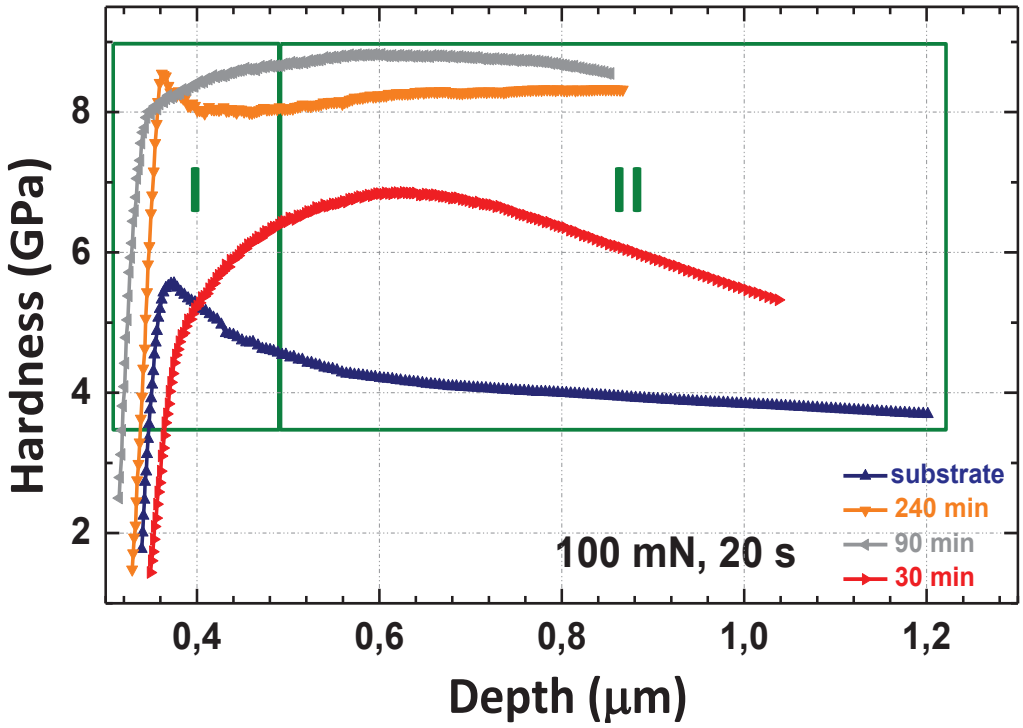

Figure 3.8. Relationship between dynamic micro-hardness from the surface for the un-implanted and N ion implanted layer at different process times which are 30 min, 90 min, and 240 min.

Nanohardness and microhardness data table show the similar results. Hardness behavior scales up four times at 240 min for 30 mN. Low load peak can be ignored such as 9 mN. Because the rise is really high.

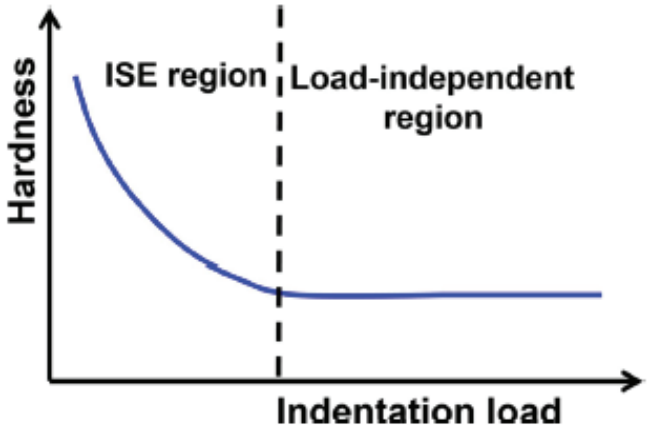

Figure 3.9. Schematic diagram of indentation size effect (ISE) [63]

Micro hardness results show that increasing of hardness is more than twice from substrate to treated surface. On the other hand, nano indentation datas indicate that hardness go up more than fourth. Because micro hardness test was applied after implantation process and before nano indentation test, surface preparation which are grinding and polishing steps were done cross section sample. Mechanical polishing can lead the deformation as like work hardening [49].

3.3. Nitrogen Depth Profiling

Nitrogen concentration profiles of the N implanted 316 SS samples were obtained by SIMS as a function of depth. Figure 3.10 show SIMS results of nitrogen implanted 316 SS samples at different processing times which are 30, 90, 240 in turn. The nitrogen concentration values are pretty high at the surfaces of N implanted samples (ranging from ~20 to ~35 at % for 316 SS). At low processing time (30 min), N profile start decrease rapidly for the samples, while at higher processing times (90, 240 min), they decrease slowly to a level of ~15 at.% and then decrease exponentially. The diffusion depth value reaches about max 8 μm at 240 min, whereas the diffusion depth at 30 min and 90 min are about 4 and 7 μm for the same treatment temperature, respectively.

To construe with cut in three sections of SIMS data, it can be seen clearly from the Region I (first 2 μm), profile of 30 min decrease slowly and profile of 90 min show constant distribution about 28 at %, although profile of 240 min start from 20 at % and increase to 32 at %. This behavior of profile can explained about sputter effect of ion implantation process due to extended period of time.

At Region II, comparison of the nitrogen depth profiles for 90 min and 240 min presents a similar nitrogen distribution and decreasing ratios are same ways. Unlike both of them, profile of 30 min reduced sharply and run shorting of nitrogen at 4 μm. Finally, there is not intensity about profile of 30min. Second profile which is treated at 90 min disappears at 7 μm in depth. Despite all, profile of 240 min continue end of 8 μm with 32 at % nitrogen distribution.

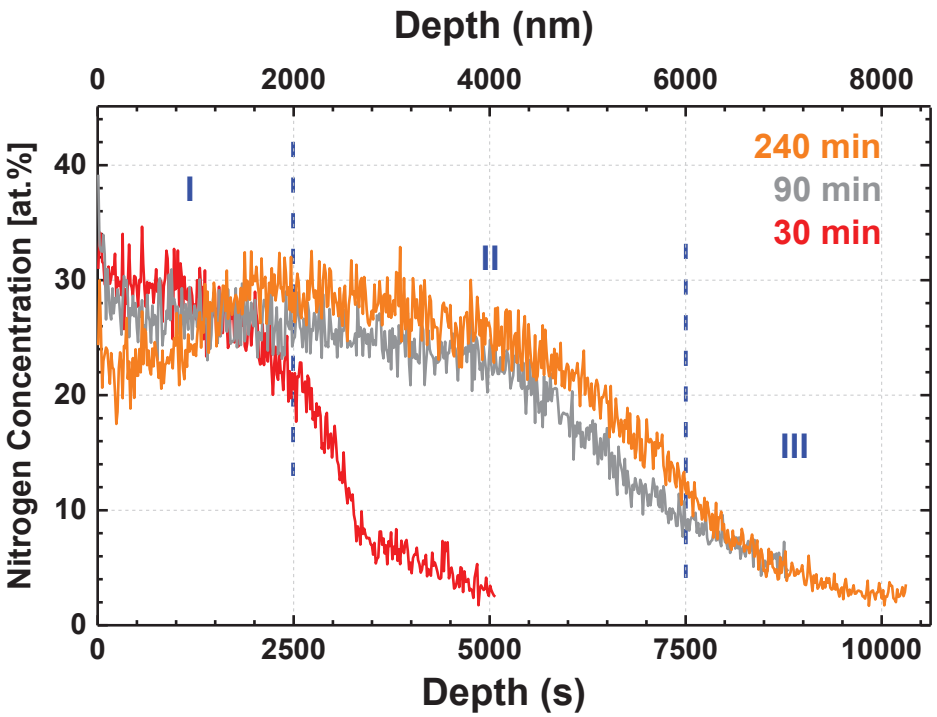

Figure 3.10. SIMS nitrogen depth profiles for N implanted 316 samples which is treated at 30 min, 90 min, and 240 min.

3.3.1 Cross Section Profile with SEM

Cross-sectional characterization of the N implanted 316 SS specimen which is treated 240 min, were carried out by using SEM. The cross-sectional sample preparation is identify in the materials and experimental methods (Chapter 2). The goal of the cross-sectional characterization is mainly to determinate the N implanted layer thicknesses as well as to investigate the expanded phases of treated layer. In addition, data results are understood consistence with SIMs profile.

Increasing the time, nitrogen concentration was fast growth. Based on the EDX and BSEM datas, γ_N layer thickness is at least 5 µm for 240 min sample.

The average thicknesses of the N implanted layers for 240 min obtained from cross-sectional SEM - EDX analyze is at least 5 µm shown in Figure 3.11.a. There is interference approximately 7.8 µm that is consisting of bakalite material because of sample preparing shown in Figure 3.11.b .BSED image show the nitrogen implanted phase distribution as very well and thickness is approximately 4,5 µm like EDX. In addition, mapping image support the result of EDX and BSED.

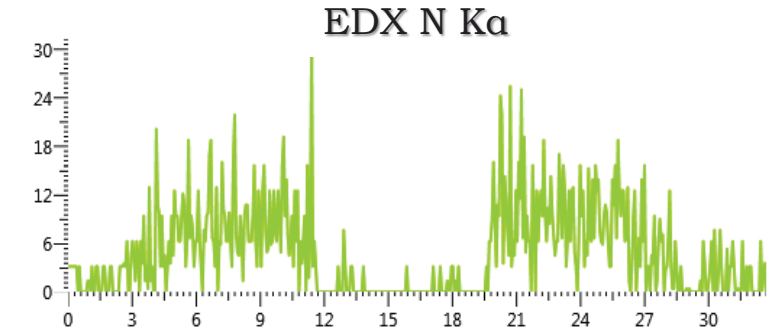

a

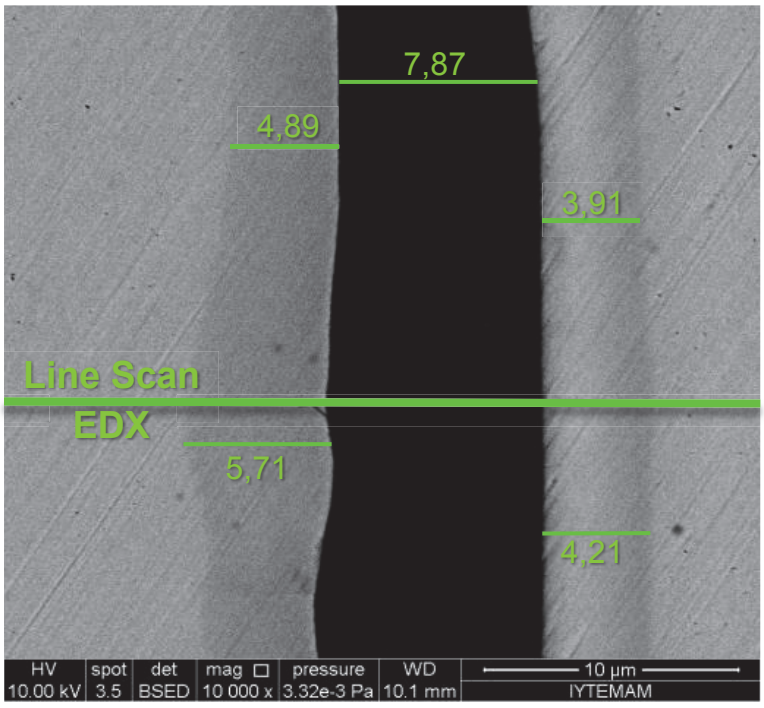

b

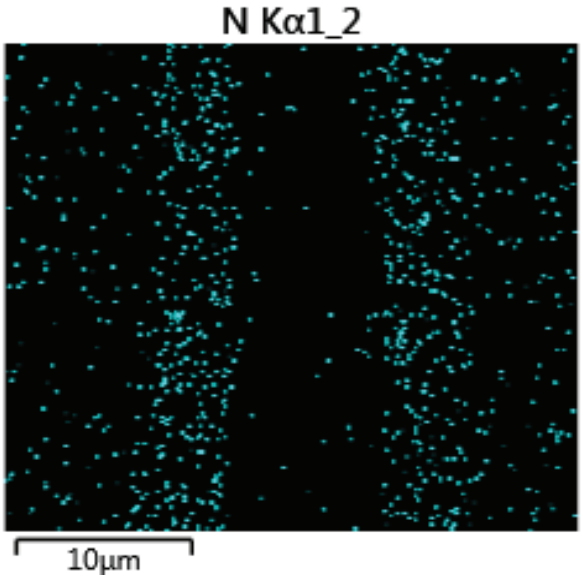

c

Figure 3.11. Actual SEM result of Nitrogen profile distribution for cross section sample which is treated 240 min (a) EDX, (b) BSEM, (c) Mapping.

3.4. Expanded Austenite Phase

Primarily analyzing to interstitial emplacement of nitrogen effect into the near-surface crystal structure of ion implanted surface was practiced with Gonio X-ray diffraction method. The XRD patterns are shown in Figure 3.12 to paraphrase that substrate γ-SS peaks and γ_N peaks which are treated at different times (30 min, 90 min, and 240 min).

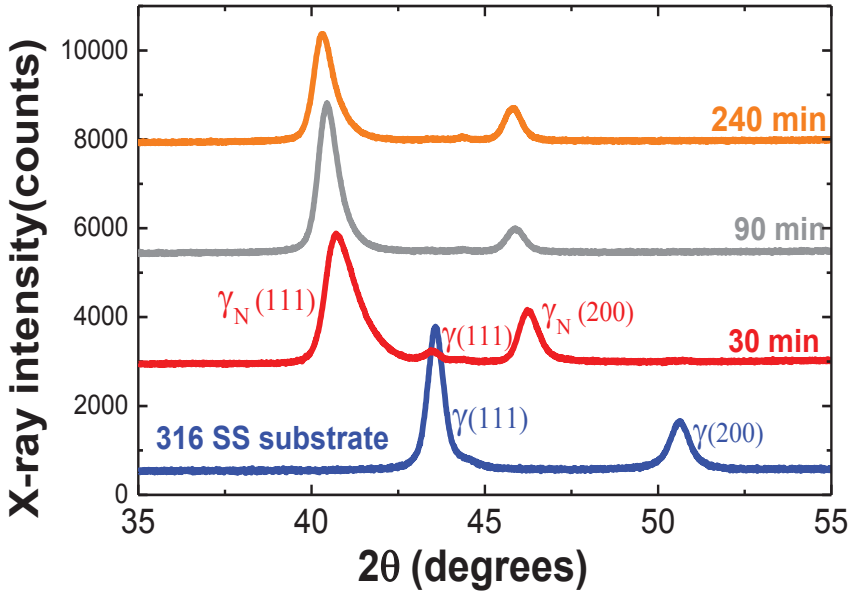

Figure 3.12. XRD Gonio patterns of substrate and Nitrogen implanted 316L SS samples which are treated at 30 min, 90 min and 240 min.

It has been an experimented thing that the common intentsities of the (111) and (200) peaks for the substrate γ-SS [27]. Data shows the formation of expanded austenite phase, (200) γ_N peak is shifted more than (111) γ_N peak suggesting grain-dependent N content behaviour. In addition, N fasten really deep way into the grain and (200) γ_N planes are oriented parallelly [27]. In Table 3.1, it can be clearly seen that N content is larger for each processing time in the (200) oriented grains. The crystalline structure of this expanded phase is not clarified. It is in substantial agreement that the lattice expantion occurred by internal stress. Some researches have shown that the diffraction peaks of expanded phase are scaled up with the increasing of treatment time to 60 min [64] like in our study shown in Figure 3.12. However, the intensity of (111) γ_N is decreased at 240 min.

Figure 3.13 a and b indicate the ideal fcc-like structure. Nitrogen atoms can be placed at octahedral (200) γN and tetrahedral (111) γN sides. All the process with

different times shows that nitrogen atoms can be located at octahedral sides than tetrahedral sites [64].

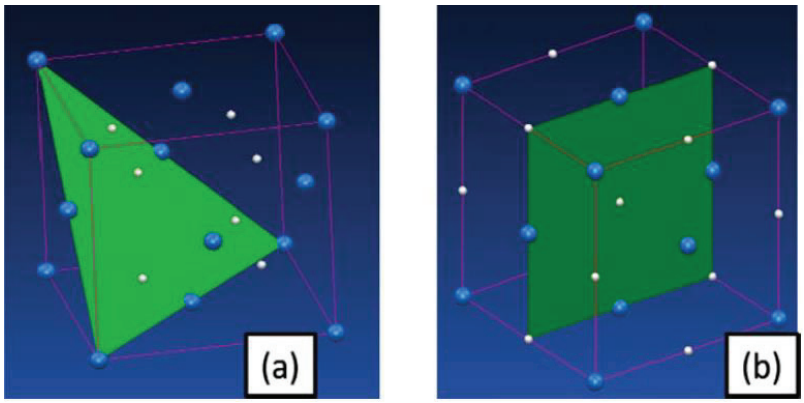

a b

Figure 3.13. Schematic drawings of nitrogen atoms on tetrahedral (a) and octahedral (b) plane [64]

Literature reviews indicate that (220) , (311) and (222) planes when Bragg angle scanning range is from 65° to 100° for substrate (γ-SS) and expanded phases (γN). Nevertheless, the lattice expansion is apeared slightly for (220) , (311) and (222) planes compared with the (200) plane. For that reson, N content is calculated based on (200) and (111) peak positions, values of 28 at. % and 40 at. % in orderly are attain a result.

Table 3.2. Lattice parameters, d and a, θ for the 3 6L fcc substrate and fcc γ_N phases. Δa/a refers to the relative difference in lattice spacing.

Implantation time	**Phase**	**2θ**	**d**	**Lattice constant a**	**<a>**	**Lattice expansion**
(min.)		***(degrees)***	***(Å)***	***(Å)***	***(Å)***	***Δa/a (%)***
Substrate	γ_{111}	43,583	2,075	3,59	3,60	-
	γ_{200}	50,623	1,802	3,60		
30	γ_{N111}	40,816	1,960	3,83	3,87	6,7
	γ_{N200}	46,274	2,080	3,92		8,9
90	γ_{N111}	40,484	2,226	3,86	3,90	7,5
	γ_{N200}	45,876	1,977	3,95		9,7
240	γ_{N111}	40,360	2,233	3,87	3,91	7,8
	γ_{N200}	45,807	1,979	3,96		10

3.5. Origin of Hardness

Expanded austenite phase consists of metastable interstitally solid solution of nitrogen and surface morphology changes induced by the nitrogen implantation. Deformation on the surfaces of specimens increases as the process time increases.

In Figure 3.14 a very fine and homogenous grain structure of surfaces is clearly seen. The images clearly reveal the grain structure of the N implanted layers. Periodic arrays of lines on the nitrided surface indicating the presence of slip bands inside the grains due to strain resulting from high nitrogen contents in the γ_N layer because of solid solution strenghtening.

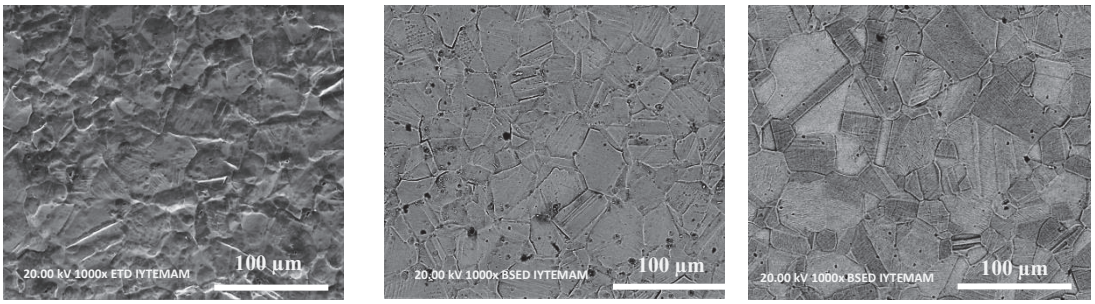

240 minutes 90 minutes 30 minutes

Figure 3.14. Topographical SEM images of (a) 240 minutes nitrogen ion implanted, (b) 90 minutes nitrogen ion implanted, (c) 30 minutes nitrogen ion implanted specimens.

CHAPTER 4

CONCLUSION

Structural and nanohardness behaviour of expanded austenite layers on austenitic stainless steel produced by ion implantation process are reported. Nanoindentation hardness is applied on the cross section of the nitrogen implanted 316L SS sample for 240 min. Surface microhardness values are obtained from samples which are treated 30, 90 and 240 min. The results show the hardness increases for all of the nitrogen implanted samples. Nitrogen concentration was investigated with SIMS and SEM methods. All methods show that 90 and 240 min have good hardness and concentration with near each other. XRD result indicate that octahedral interstital positions include nitrogen atoms.

In addition,The nitrogen ion implanted layers are composed of high-N content phase γ_N - (Fe, Cr, Ni). Average N content was found between 8-10 at %. Thickness of the nitrogen implanted layer was found ranging from 4 to 8 micron. The results showed that the hardness increased for all the nitrogen implanted samples. All methods showed that 90 and 240 min have good hardness and concentration with near each other. XRD result indicated that the octahedral interstitial positions include nitrogen atoms.

REFERENCES

[1] J. Black, G. Hasting, Handbook of Biomaterial Properties, Champain & Hall, 1998, 135-165.

[2] E. Menthe and K.T. Rie: Surface and Coatings Technology, 1999, 116-119, 199-204.

[3] https://malinco.com/medical-wire/.

[4] D.L. Williamson, Li Wang, R. Wei, P.J. Wilbur, Mater. Lett. 9, 27 (1990).

[5] Ferguson, A.B., Akahashi, Y., Laing, P.G. and Hodge, E.S. (1962) /. Bone and Joint Surg., 44, 323.

[6] Hildebrand, H.F., Mercier, J.V., Decaeslecker, A.M., Ostapzuk, P., Stoeppler, U., Roumazeille, B. and Decloulx, J., Biomaterials.

[7] Breme, J. Steinhauser, E. and Paulus, G. (1988) Commercially Pure Titanium Steinhauser Plate-Screw System for Maxillo facial Surgery. Biomaterials, 9, 310-313.

[8] R. A. Vieira, M. C. A. Nono, and N. C. Cruz, Nanohardness of a Ti Thin Film and Its Interface Deposited by an Electron Beam on a 304 SS Substrate, Phys. Stat. Sol.,232,No.1, 116-120 (2002).

[9] I. Chen, X.Y. Li, T. Bell, H. Dong, Improving the wear properties of Stellite 21 alloy by plasma surface alloying with carbon and nitrogen, Wear 264 (2008) 157–165.

[10] T. Bell, Current Status of Supersaturated Surface Engineered S-phase Materials, International Heat Treatment and Surface Engineering, 1:4, 148-151, 2007.

[11] W. Betteridge, Cobalt and Its Alloys, Chicester: Horwood Publishing, New York, 1982.

[12] P. Crook, Cobalt and Cobalt Alloys, ASM Handbook, Vol.2: Properties and Selection: Nonferrous Alloys and Special-Purpose Material, 1992.

[13] O. Öztürk, Microstructural and mechanical characterization of nitrogen ion implanted layer on 316L stainless steel, Nuclear Instruments and Methods in Physics Research B 267 (2009) 1526–1530.

[14] S. Williams, I. M. Poate, Ion Implantation and Beam Processing, Academic Press Australia, 1984, 1-40.

[15] T. Christiansen and M.A.J. Somers, On the crystallographic structure of S-phase, Scripta Materialla, 2004, 50, 35-37.

[16] T. Christiansen, M. A. J. Somers, Characterization of low temperature surface hardened stainless steel, Struers Journal of Materialography 9, 2006.

[17] Y. Sun, X. Li and T. Bell, Material Science and Technology, 1999, 15, 1171-1178.

[18] Y. Sun, T. Bell, Z. Kolosvary and J. Flis, Heat Treatment of Metals, 1999, 1, 9-16.

[19] C. Blawert, H. Kalvelage, B.L. Mordike, G.A. Collins, K. T. Short, Y. Jiraskova and O. Schneeweiss, Surface and Coatings Technology, 2001, 136, 181-187.

[20] Z. L. Zhang and T. Bell: Proc. 3rd Int. Cong. on 'Heat treatment of materials', Shanghai, China, November 1983, The Metals Society.

[21] T. Christiansen, M. A. J. Somers, Decomposition kinetics of expanded austenite with nitrogen contents, Zeitschrift für Metallkunde, in press.

[22] X.Y. Li, Y. Sun and T. Bell: Stability of the nitrogen S-phase in austenitic stainless steel, Z. Metallkd., 1999, 90(11), 901-907.

[23] Y. Jiraskova, C. Blawert and O. Scheeweiss: Thermal Stability of Stainless Steel Surfaces Nitrided by Plasma Immersion Ion Implantation, Phys. Stat. Sol. (a), 1999, 175, 537-548.

[24] D.L. Williamson, O. Ozturk, S. Glick, R. Wei and P.J. Wilbur, Microstructure of ultrahigh dose nitrogen-implanted iron and stainless steel, Nuclear Instruments and Methods in Physics Research, B59/60 (1991), 737-741.

[25] O. Ozturk, D.L. Williamson, Phase and composition depth distribution analyses of low energy, high flux N implanted stainless steel, J. Appl. Phys. 77 (8), 1995.

[26] http://blog.bodycote.com/2017/06/18/expanded-austenite-s-phase/

[27] D.L. Williamson, O. Ozturk, R. Wei and P.J. Wilbur, Metastable phase formtaion and enhanced diffusion in f.c.c. alloys under high dose, high flux nitrogen implantation at high and low ion energies, Surf. Coat. Technol. 65, 15 (1994).

[28] R. Wei, B. Shogrin, P.J. Wilbur, O. Ozturk, D.L. Williamson, I. Ivanov, and E. Metin, J. Tribology 116, 870 (1994).

[29] X.Y. Li: Low Temperature Plasma Nitriding Of 316 Stainless Steel – Nature Of S Phase And Its Thermal Stability, Surface Engineering, 2001, 17(2), 147-152.

[30] C. A. Figueroa, D. Wisnivesky, P. Hammer, R. G. Lacerda, R. Droppa, Jr. F. C. Marques, F. Alvarez, A comprehensive nitriding study by low energy ion beam implantation on stainless steel, Surface and Coatings Technology, Volumes 146–147, September–October.

[31] E. Mene´ndez, A. Martinavicius, M.O. Liedke, G. Abrasonis, J. Fassbender, J. Sommerlatte, K. Nielsch, S. Surin˜ach, M.D. Baro, J. Nogue´s, J. Sort, Patterning of magnetic structures on austenitic stainless steel by local ion beam nitriding, Acta Materiali.

[32] D Hoeft, B ALatella, K T Short, Residual stress and cracking in expanded austenite.

[33] D. Manova, J.W. Gerlach, F. Scholze, S. Mändl ⁎, H. Neumann, Nitriding of austenitic stainless steel by pulsed low energy ion implantation, Surface & Coatings Technology 204 (2010) 2919–2922.

[34] Oliver W, Pharr G, An improved technique for determining hardness and elastic modulus using load and displacement sensing indentation experiments, J. Mater. Res., 7(1992), 1564.

[35] R. Saha, W. D Nix, Effects of the substrate on the determination of thin film mechanical properties by nanoindentation, Acta Materialia 50 (2002) 23–38.

[36] Y. Liu, L. Li, M. Xua, X. Cai, Q. Chena, Y. Hua, P. K. Chuc, Effects of nitrogen ion implantation and implantation energy on surface properties and adhesion strength of TiN films deposited on aluminum by magnetron sputtering, Materials Science and Engineering A 415 (2006) 140–144

[37] H.S. Khatak, B Raj, Corrosion of Austenitic Stainless Steel: Mechanism, Mitigation and Monitoring, 2002, 1-33.

[38] J. Ryl, A. Arutunow, M. T. Tobiszewski and J. Wysocka, Aspects of intergranular corrosion of AISI 321stainless steel in high-carbon-containing environments, Anti-Corrosion Methods and Materials 61/5 (2014) 328–333

[39] J.C.M. Farrar, The alloy tree A guide to low-alloy steels, stainless steels and nickel-base alloys, 2004, 74-75.

[40] G.S. Was, Ion Beam Modification Of Metals: Compositional And Microstructural Changes, Progress in Surface Science, 32(1990), 211-332.

[41] P. J. Wilbur, R. Wei, High-current-density metal-ion implantation, Review of Scientific Instruments 63, 2491 (1992).

[42] D.L Williamson, P.J. Wilbur, F.R. Fickett, S. Parascandola, Role of ion-beam processing time in the formation and growth of the high-nitrogen phase in austenitic stainless steel, BOOK-INSTITUTE OF MATERIALS. 2001, Vol. 752, pp. 333-352.

[43] O'NeiU, Hugh ,Hardness Measurements of Metals and Alloys, Chapman & Hall, London, 1967

[44] Tabor, D., 1951, The Hardness of Metals, Oxford University Press, London.

[45] G. Subhash, B. J. Koepper, A. Chandra, Dynamic Indentation Hardness and Rate Sensitivity in Metals, Journal of Engineering Materials and Technology, JULY 1999, Vol. 121 / 257-262

[46] Wang, Influences of sample preparation on the indentation size effect and nanoindentation pop-in on nickel, University of Tennessee, 2012.

[47] P. B. F. Soares, S. A. Nunes, S. D. Franco, R. R. Pires, D. Zanetta-Barbosa, C. J. Soares, Measurement of Elastic Modulus and Vickers Hardness of Surround Bone Implant Using Dynamic Microindentation – Parameters Definition, Brazilian Dental Journal (2014) 25(5): 385-390

[48] A.C. Fischer-Cripps, Critical review of analysis and interpretation of nanoindentation test data, Surface Coatings Technologies 200 (2006) 4153-4165.

[49] Wang, Influences of sample preparation on the indentation size effect and nanoindentation pop-in on nickel, University of Tennessee, 2012.

[50] Alpha Laser Inc. http://alphalasercutting.com/water-jet/

[51] ME 3701, Materials of Engineering, LSU, sample preparation notes, http://imechanica.org/files/handout9.pdf.

[52] Struers Inc. https://www.struers.com/en/Knowledge/Mounting/Hot-mounting

[53] Oliver W, Pharr G, An improved technique for determining hardness and elastic modulus using load and displacement sensing indentation experiments, J. Mater. Res., 7(1992), 1564.

[54] B. D. Cullity, S. R. Stock, Elements of X-Ray Diffraction (3rd Edition), 1956, 1-23.

[55] R. G. Wilson, F. A. Stevie, and C. W. Magee, Secondary Ion Mass Spectrometry – A Practical Handbook for Depth Profiling and Bulk Impurity Analysis, Wiley Interscience, 1989.

[56] Secondary ion mass spectrometry (sims) - The University of Edinburgh. http://www.ed.ac.uk/files/atoms/files/sims4.pdf.

[57] Ray F. Egerton, Physical Principles of Electron Microscopy An Introduction to TEM, SEM, and AEM, Springer Science+Business Media, 2005, 17-167.

[58] Y. Choi, K.J. Van Vliet, J.Li,S. Suresh; J. Appl. Phys. 94 (2003) 6050.

[59] W. F. Smith, Principles of Materials Science and Engineering 3 (1996), 249-326.

[60] Y.I. Golovin, Physics of the Solid State (2008) 2205.

[61] L. Min, C. Weimin, Factors Resulting in Micron Indentation Hardness Descending in Indentation Tests, Chinese Journal of Aeronautics 22(2009) 43-48

[62] H. Wua, Y. Lia, X. Tanga, G. Hussainb, H. Zhaoa, Q. Lia, A. Adedotunba, Nano-mechanical characterization of plasma surface tungstenizedlayer by depth-sensing nano-indentation measurement, Applied Surface Science 324 (2015) 160–167.

[63] E. Broitman, Indentation Hardness Measurements at Macro-, Micro-, and Nanoscale: A Critical Overview, Tribol Lett (2017) 65:23

[64] R.L.O. Basso; V.L. Pimentel; S. Weber; G. Marcos; T. Czerwiec; I.J.R. Baumvol; Magnetic and structural properties of ion nitrided stainless steel, Journal of Applied Physics,105, 124914, 2009.